Dalton Transactions

PAPER

View Article Online
View Journal | View Issue

Open Access Article. Published on 26 February 2016. Downloaded on 20/04/2016 08:56:07.
This article is licensed under a Creative Commons Attribution 3.0 Unported Licence.

Cite this: *Dalton Trans.*, 2016, **45**, 6893

Role of crystal size on swing-effect and adsorption induced structure transition of ZIF-8†

Tian Tian,[a] Michael T. Wharmby,[b] José B. Parra,[c] Conchi O. Ania[c] and David Fairen-Jimenez*[a]

Received 9th February 2016,
Accepted 25th February 2016

DOI: 10.1039/c6dt00565a

www.rsc.org/dalton

The flexibility and structure transition behaviour of ZIF-8 in a series of samples with different particle size has been studied using a combination of high-resolution N_2 gas adsorption isotherms and, for the first time, a broad *in situ* PXRD and Rietveld analysis. During the stepped adsorption process, large particles showed a narrow adsorption/desorption pressure range with a shorter equilibrium time due to lower kinetic hindrance, deriving from higher amount of active sites. *In situ* PXRD showed that both the rotation of imidazole ring and a bend in the methyl group led to the gate opening of ZIF-8.

Introduction

Zeolitic imidazole frameworks (ZIFs) are a subfamily of metal–organic frameworks (MOFs) with zeolitic topologies. ZIFs have attracted great interest for combining the advantages of MOFs (*i.e.* large pore volume, high surface area, tuneable chemical functionality) and zeolites (*i.e.* high thermal and chemical stability).[1] These properties make ZIFs excellent candidates in gas adsorption,[2,3] separation[4,5] and catalysis.[6,7]

Among all ZIFs, ZIF-8 [$Zn(mIM)_2$] (mIM = 2-methylimidazolate, $C_4H_5N_2^-$) is of particular interest due to its high thermal and chemical stability, and characteristic porosity.[8,9] ZIF-8 presents a large BET area (S_{BET} *ca.* 1700 $m^2\ g^{-1}$) and relative high crystal densities (0.95 g cm^{-3}), and can be prepared in large and chemically robust monolithic morphologies with large volumetric adsorption capacities (S_{BET}(vol) = 1660 $m^2\ cm^{-3}$).[10] ZIF-8 possesses a sodalite (SOD) topology containing relatively large pore cavities (*ca.* 11.6 Å diameter) interconnected by small windows (*ca.* 3.4 Å diameter).[11] Due to its small window size, ZIF-8 was expected to separate molecules with different kinetic diameters. However, it was found that gas molecules with diameter larger than 3.4 Å, *e.g.* N_2 (3.6 Å), could also be adsorbed.[12]

In a previous study, we combined the use of grand canonical Monte Carlo (GCMC) simulations and *in situ* powder X-ray diffraction (PXRD) to demonstrate that the structural transition of ZIF-8 was induced by gas adsorption, from an ambient to a high pressure structure, ZIF-8AP and ZIF-8HP, respectively.[13] The structural change implies the reorientation of the mIM ligands and the increase in the size of both the 4- and 6-ring windows present in this material. In particular, the *swing effect* of the imidazole rings is responsible for the stepwise adsorption of N_2 at 77 K at 0.02 p/p_0. We have also shown the existence of the *swing effect* and phase transition in ZIF-8 during the adsorption of other alkanes at *ca.* 0.1 p/p_0 and 125 K for methane; as well as 0.3 p/p_0, 0.02 p/p_0 and 6×10^{-3} p/p_0 at 273 K for ethane, propane and butane, respectively.[14] Interestingly, in all these later cases the phase transition takes place without observing a stepped behaviour in the adsorption process (*i.e.* Type I adsorption isotherms). Using DFT calculations, we showed that the driving force for this transition was related to the insertion of additional molecules in the 4-ring windows, which in turn stabilizes the "high-loading" ZIF-8HP structure. Following this work, Ania *et al.* studied the structural transition of ZIF-8 using high resolution adsorption isotherms of different gases (CO, N_2, O_2, Ar) at different temperatures (77 and 90 K) and found that polarizability, size and shape of gas molecules affected the swing effect and phase transition behaviour.[15] Contrary to our previous results,[13] Ania *et al.*[15] and Park *et al.*,[1] observed hysteresis during the desorption of N_2 and Ar at cryogenic temperatures as well as some other gases such as CO and O_2, and reported the existence of two adsorption substeps around the transition pressure, attributing this behaviour to the reorganization of the adsorbed gas molecules and their interactions with the framework. In addition to these studies, the swing effect of ZIF-8 has been further studied both experimentally and computationally.[16,17] For example, by using single crystal XRD and Raman spectroscopy, it has been observed that the structural transition of

[a]*Department of Chemical Engineering and Biotechnology, University of Cambridge, Pembroke St., Cambridge CB2 3RA, UK. E-mail: df334@cam.ac.uk*
[b]*Diamond Light Source Ltd., Diamond House, Harwell Science & Innovation Campus, Didcot, Oxon., OX11 0DE, UK*
[c]*Instituto Nacional del Carbón, INCAR-CSIC, Oviedo, Spain*

† Electronic supplementary information (ESI) available: Particle size distribution, gas adsorption, BET areas calculation, and *in situ* X-ray diffraction. See DOI: 10.1039/c6dt00565a

Open Access Article. Published on 26 February 2016. Downloaded on 20/04/2016 08:56:07.
This article is licensed under a Creative Commons Attribution 3.0 Unported Licence.

ZIF-8 was also induced by reducing the temperature beyond 150 K under N_2.[18,19] We and others have also shown recently the use of THz radiation and inelastic neutron scattering for the study of the flexibility modes of ZIF-8.[20–22] Although the adsorption mechanism of multiple gases as well as the shape of the adsorption isotherms of ZIF-8 have been widely investigated, the origin of the substeps in the adsorption isotherms of various gases at cryogenic temperatures, and of the occurrence of a hysteresis loop during the desorption are still unclear.

During the preparation of this manuscript, Zhang *et al.* demonstrated that the particle size of ZIF-8 affected its structural transition during N_2 adsorption at 77 K.[23] By applying the osmotic framework adsorbed solution theory (OFAST),[24] they observed that the pressure for the phase transition shifted to higher values when the particle size was reduced. This finding is especially relevant because ZIF-8 can be synthesized with particle sizes in the nanometre to micrometre range.[25] In this regard, the flexibility of ZIF-8 is of particular importance as it affects the diffusivity of gas molecules through the porous network. Indeed, previous molecular dynamic studies have shown tremendous differences in the diffusivity of gas molecules between the rigid and the flexible structure of ZIF-8.[14,26,27]

In this work, we synthesised ZIF-8 with a wide range of particle sizes and studied the role of the particle size on the gas-induced structural transition on adsorption of N_2 at 77 K, as well as the kinetics of the process. We also include, for the first time, a detailed study about the mechanisms of the phase transition during the adsorption process by using *in situ* PXRD experiments during N_2 adsorption at cryogenic temperature on two different sized ZIF-8 samples.

Experimental

Materials

$Zn(NO_3)\cdot 6H_2O$ (98%), 2-methylimidazole (97%), sodium formate (98%) and methanol (99%) were purchased from Alfa Aesar. All chemicals were used as received.

Synthesis of ZIF-8s

Six different ZIF-8 samples with different particle size were prepared using different methods. ZIF-8-0.14 was synthesised based on the method reported by Pan *et al.*[28] Aqueous solutions of $Zn(NO_3)\cdot 6H_2O$ (8 ml, 0.492 M) and 2-methylimidazole (80 ml, 3.46 M) were mixed and stirred for 5 minutes under ambient conditions.

ZIF-8-0.21, ZIF-8-0.61 and ZIF-8-1.6 were synthesised based on methods reported by Kida *et al.*[29] Aqueous solutions of $Zn(NO_3)\cdot 6H_2O$ (10 ml, 0.25 M) and 2-methylimidazole (90 ml, 2.77 M) were mixed and stirred for 24 h under ambient conditions to synthesise ZIF-8-0.21. ZIF-8-0.61 and ZIF-8-1.6 were synthesised by reducing the concentration of 2-methylimidazole to 1.66 M and 1.11 M, respectively, while keeping other conditions unchanged.

ZIF-8-10 and ZIF-8-98 were synthesised based on methods reported by Zhang *et al.*[30] For ZIF-8-10, 2-methylimidazole (0.099 M) and sodium formate (0.198 M) were dissolved in 40 ml of methanol, which was then poured into a solution of $Zn(NO_3)\cdot 6H_2O$ (40 ml, 0.049 M) in methanol. The mixture was placed in a Teflon-lined steel autoclave and heated at 363 K overnight. For ZIF-8-98, 2-methylimidazole (0.593 M) and sodium formate (0.281 M) were dissolved in 40 ml of methanol, and then poured into a solution of $Zn(NO_3)\cdot 6H_2O$ (40 ml, 0.3 M) in methanol. The mixture was placed in a Teflon-lined steel autoclave and heated at 363 K overnight.

All as synthesised solids were collected by centrifugation, washed with ethanol (20 ml, 3 times) and dried at 373 K under vacuum.

Characterisation of materials

Powder X-ray diffraction (PXRD) patterns were recorded with a Bruker D8 diffractometer using Cu $K\alpha_1$ (λ = 1.54056 Å) radiation with a step of 0.02° at a scanning speed of 0.1° s^{-1}. Scanning electron microscope (SEM) images were taken using a Hitachi S-5500 FE SEM with an accelerating voltage of 1 kV.

High resolution N_2 adsorption–desorption isotherms were measured at 77 K using a Micromeritics ASAP 2020 instrument in the relative pressure range from 10^{-6} to 1 for the adsorption branch and down to 10^{-3} for the desorption branch. The instrument was equipped with a molecular drag vacuum pump and three pressure transducers (0.1, 10, 1000 mmHg, uncertainty within 0.15% of reading) to enhance the sensitivity in the low-pressure range. All samples were evacuated overnight for 24 h at 423 K under dynamic vacuum prior to adsorption. Strict analysis conditions were programmed during the gas adsorption measurements to ensure equilibrium data in all cases. Consequently, the average elapsed time for the measurement of the isotherms was 90–120 h, with over 200 equilibrium points on average per isotherms. The saturation pressure of the gas was continuously measured throughout the analysis by means of a pressure transducer. For all isotherms, warm and cold freespace correction measurements were performed by using ultrahigh purity He gas (grade 5.0, 99.999% purity). Ultrahigh purity N_2 (*i.e.* 99.9992%) was provided by Air Products.

Data for the *in situ* gas adsorption powder X-ray diffraction experiments were collected at beamline I11 at Diamond Light Source (Oxon., UK; λ = 0.825701 Å), using the I11 gas cell at 80 K.[31–33] Both ZIF-8-0.14 and ZIF-8-98 samples were activated prior to the gas adsorption experiment by heating to 413 K under vacuum. Data were collected at 22 different pressures, 11 in the 0.0–0.1 p/p_0 range and 11 in the 0.1–0.9 p/p_0 range. Selected pressure points were fully refined by the Rietveld method using the TOPAS-Academic v5 suite.[34] Subsequently, these structures were used as fixed points in a parametric Rietveld refinement,[35] also performed using TOPAS-Academic v5. See ESI† for full details.

 This journal is © The Royal Society of Chemistry 2016

Open Access Article. Published on 26 February 2016. Downloaded on 20/04/2016 08:56:07.
This article is licensed under a Creative Commons Attribution 3.0 Unported Licence.

Results and discussion

ZIF-8 particle size and gas adsorption

We controlled the particle size of ZIF-8 by modifying the Zn/mIM ratio or by incorporating additives as reported elsewhere.[9,29,36] Fig. 1 shows the PXRD patterns of the different samples. The different samples matched the simulated PXRD pattern, indicating the successful synthesis of ZIF-8. Although the full width at half maximum was larger for small particles than for large ones, we were not able to calculate the particle size by using the Scherrer equation since the equipment contribution to the broadening of the Bragg peaks was larger than the contribution from the samples. In this case, we measured the particle size of ZIF-8 samples by using SEM. Fig. 2 shows the SEM images, whilst Fig. S1† and Table 1 show the normal (Gaussian) distribution and the average particle size, respectively, of the different ZIF-8 samples. Particle size for ZIF-8 was in the range between 0.141 and 98 μm. In particular, smaller particle size ZIF-8 showed narrower size distribution compared with larger ones.

We further analysed the porosity for all samples by using high-resolution N_2 adsorption/desorption isotherms at 77 K. The BET areas of ZIF-8 samples were calculated using the Rouquerol's consistency criteria.[37] Table 1 shows similar BET areas, ranging between 1700 and 1810 $m^2\ g^{-1}$, for all the materials. Fig. 3 shows the adsorption isotherms of N_2 on ZIF-8 samples; we used a semi-log plot to give more detail in the low pressure range. All samples presented the same characteristic stepwise adsorption isotherm widely reported for ZIF-8[1,13,15] and the swing effect of the mIM rings at a similar onset transition, of *ca.* 5×10^{-3} p/p_0. As particle size decreases, the samples showed a slight increase in the uptake during the plateau and close to saturation. This effect is attributed to the existence of interstitial spaces between ZIF-8 particles, something that is more important for smaller particle size.

Fig. 3 (inset) shows a magnification of the adsorption isotherms in the phase transition region for clarity, whereas

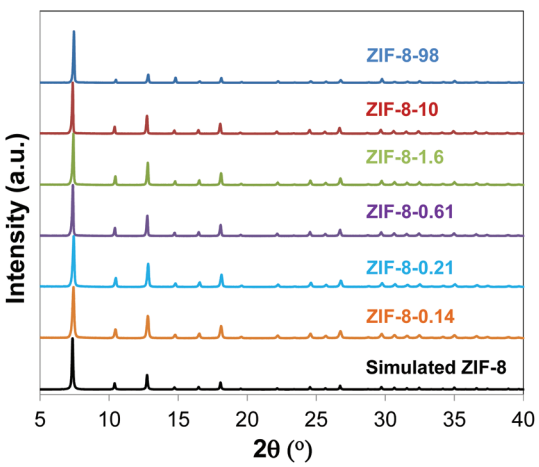

Fig. 1 PXRD patterns of ZIF-8 with a different particle size alongside a simulated ZIF-8.

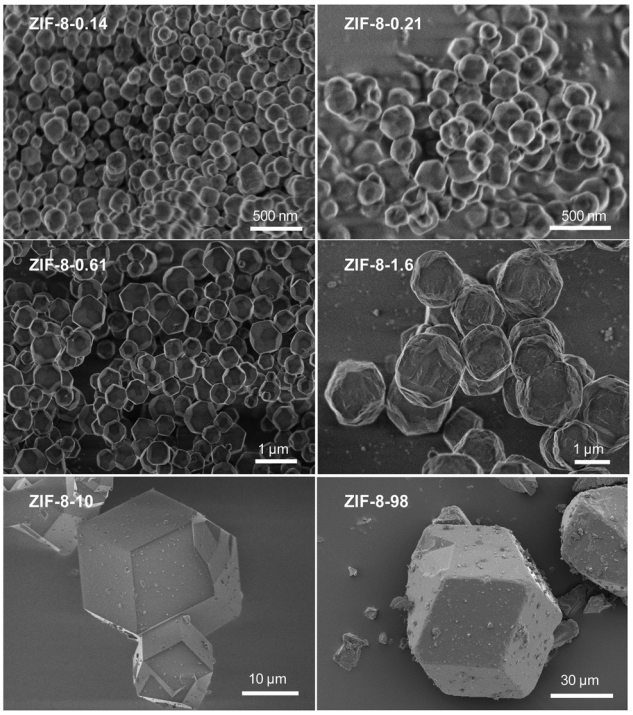

Fig. 2 SEM images of ZIF-8 with a different particle size.

Table 1 Particle size and BET areas of ZIF-8 with different particle size

Materials	Particle size (μm)	BET areas ($m^2\ g^{-1}$)
ZIF-8-0.14	0.141 ± 0.035	1740
ZIF-8-0.21	0.213 ± 0.041	1702
ZIF-8-0.61	0.608 ± 0.013	1739
ZIF-8-1.6	1.6 ± 0.4	1799
ZIF-8-10	10.0 ± 0.5	1809
ZIF-8-98	98 ± 34	1731

Fig. 4 and S4† show the adsorption and desorption branches, where the differences between samples of different size are evident. On the one hand, samples with smaller particle size (*i.e.* ZIF-8-0.14 and ZIF-8-0.21) shifted the gate pressure for the adsorption substep to higher p/p_0 values compared to samples with larger particle size (*i.e.* from 0.006 to 0.014 p/p_0). On the other hand, samples with smaller particle size showed a wider hysteresis loop compared to larger particle samples. Interestingly, in the case of ZIF-8-98 (*i.e.* the sample with the largest particle size) the adsorption was completely reversible and no hysteresis was found. These phenomena agreed well with the previous reports from Ania *et al.*, which indicate the presence of hysteresis[15] – and from some of us which show no such hysteresis.[13] As the hysteresis loop occurred at very low pressures, it cannot be explained by a capillary condensation mechanism characteristic of mesoporous materials.[38] This is attributed to the desorption of N_2 from an *opened* ZIF-8HP structure and hence gradual rearrangement of the remaining gas molecules during the transition to the initial *closed* ZIF-8AP structure.

Open Access Article. Published on 26 February 2016. Downloaded on 20/04/2016 08:56:07.
This article is licensed under a Creative Commons Attribution 3.0 Unported Licence.

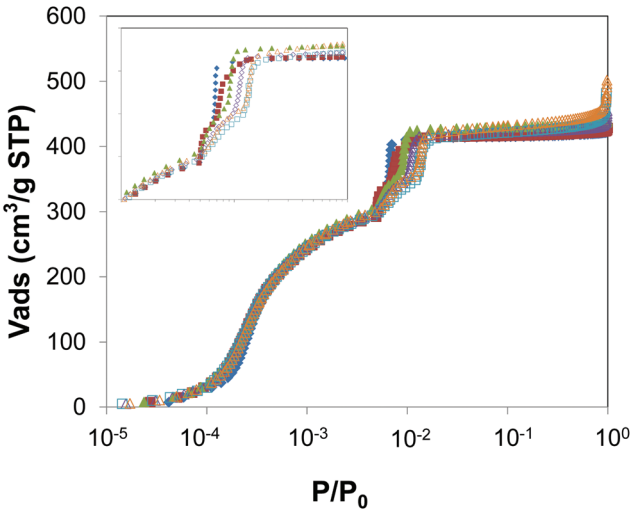

Fig. 3 Semi-log plot of N_2 adsorption isotherms at 77 K in ZIF-8 samples with different particle size. Blue closed diamonds, ZIF-98; red closed squares, ZIF-8-10; green closed triangles, ZIF-8-1.6; purple open diamonds, ZIF-8-0.61; blue open squares, ZIF-8-0.21; orange open triangles, ZIF-8-0.14.

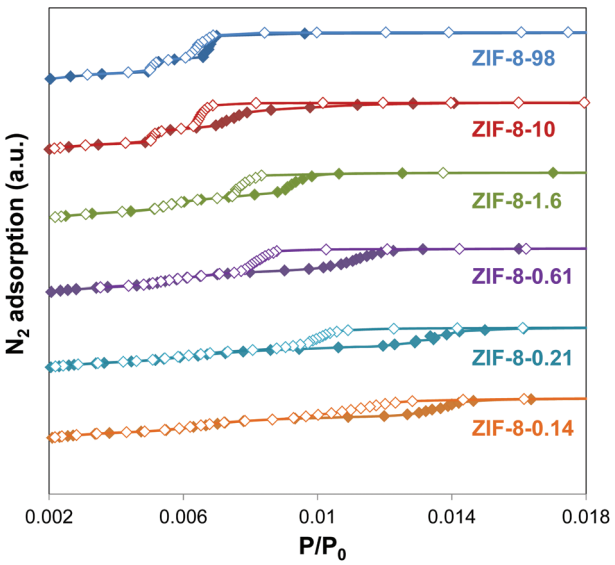

Fig. 4 Low pressure hysteresis loops of ZIF-8 samples with different particle size. Closed symbols, adsorption; open symbols, desorption.

The shift of the gate pressure to higher values and the wider range of the hysteresis loop for smaller particles suggests a higher energy barrier between ZIF-8AP and ZIF-8HP structures, and thus, a higher kinetic hindering. A similar observation was made by Watanabe *et al.*,[39] using GCMC simulation, where they showed that the width of the hysteresis loop was inversely proportional to the energy barrier. This transition was also observed experimentally by Sakata *et al.*[40] for the interpenetrated $[Cu_2(bdc)_2(bpy)]_n$ (bdc = 1,4-benzenedicarboxylate, bpy = 4,4′-bipyridine) system, which exhibited a cooperative guest-induced structural transformation from a non-porous closed phase to an open phase.

Dynamic adsorption measurements

Changes in framework flexibility are especially relevant for ZIF-8, where the very narrow windows will allow (or not) the adsorption of larger molecules. Having a range of samples with different adsorption behaviour at thermodynamic equilibrium conditions in the adsorption isotherms, we decided to study the adsorption kinetics by measuring the equilibration time of each equilibrium adsorption point of the isotherms. For clarity, Fig. 5 shows a comparison of the samples with large (*i.e.* ZIF-8-98) and small (*i.e.* ZIF-8-0.14) particle size only. Fig. S5† shows the adsorption equilibration time during the N_2 adsorption isotherm at 77 K, for all the samples.

There are three clear ranges taking into account the phase transition occurring at a gate pressure of *ca.* 5×10^{-3} p/p_0. First, before the gate pressure, all the ZIF-8 samples showed very different adsorption kinetics, with the equilibration process being much faster for samples with larger particle sizes (*e.g.* ZIF-8-98, *ca.* 25 min) than for those with smaller particle size (*e.g.* ZIF-8-0.14, ranging from 100 to 25 min). Second,

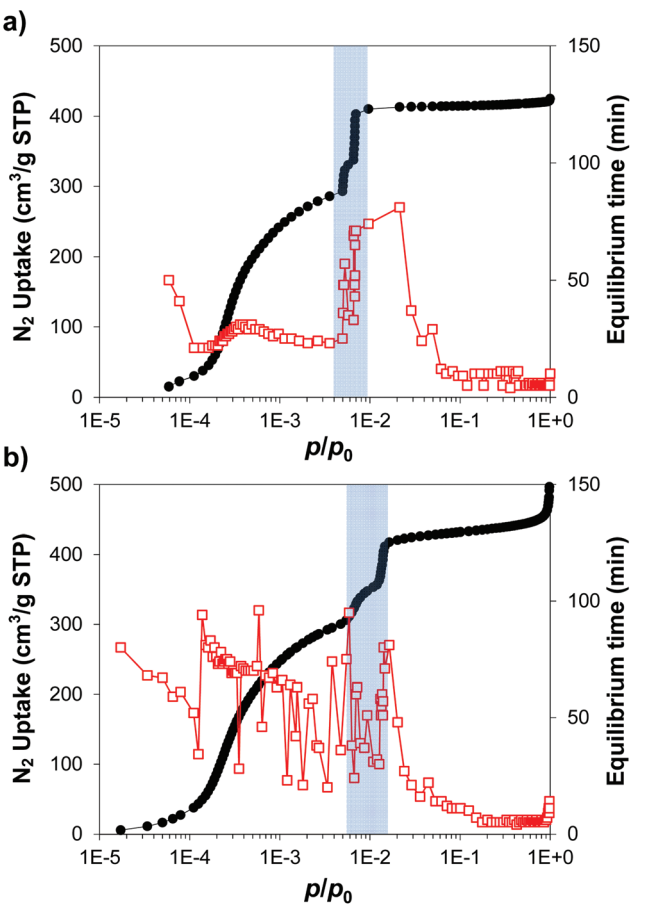

Fig. 5 Adsorption isotherms and equilibrium time for N_2 at 77 K for (a) ZIF-8-98 and (b) ZIF-8-0.14. Black circles, N_2 uptake; red empty squares, equilibrium time; grey shading, gate pressure region.

This journal is © The Royal Society of Chemistry 2016

Open Access Article. Published on 26 February 2016. Downloaded on 20/04/2016 08:56:07.
This article is licensed under a Creative Commons Attribution 3.0 Unported Licence.

the adsorption rate for all samples was significantly slowed near the gate pressure (up to *ca.* 80 min), before increasing at $p/p_0 > 0.01$ (*i.e.* after the transition to ZIF-8HP), which is the third stage with all the samples behaving similarly, with faster kinetics than at lower pressures. The dependency of the adsorption equilibration time and particle size before the gate pressure implies differences in ZIF-8AP flexibility (*i.e.* the dynamic, free swing of the mIM rings to allow access of large molecules into the cavities) between different samples at these conditions. In turn, the increase of the equilibration time (*i.e.* slow kinetics) at the gate pressure would be explained by the permanent swing of the mIM rings, and the access and rearrangement of the gas molecules in the cavities, and therefore the phase transition of ZIF-8AP to ZIF-8HP observed within this pressure range.[13] Above the transition pressure all samples present somewhat similar kinetics due to the opened structure. These observations are consistent with a model in which, below the gate pressure, the 3.4 Å windows in ZIF-8 change between open and closed configurations depending on environmental pressure gradient; whereas above the gate pressure, the windows remain open. In these conditions of static low and high pressure, a snapshot of the ZIF-8 structure would reveal (at least) two discrete, non-disordered phases ZIF-8AP and ZIF-8HP rather than a free swing of the mIM rings. This dynamic opening and closing process during the pressure swing depends on the particle size of ZIF-8.

Assuming that both the large and the small particles have the same structure, we are effecting the same change in both samples. From a thermodynamic point of view, the energy change should also be the same for both. As shown above, we found however important differences between samples, so the question would be: are there any differences in the composition or the structure of the different ZIF-8 crystals? The main difference is related to the ratio of external surface *vs.* bulk phase, which is much larger for smaller than for larger particles. This would imply that the external surface/bulk ratio of the 4-ring windows in large particles sizes is lower than in small particles. If the driving force for the phase transition is the adsorption of additional N_2 molecules in the 4-ring window in the bulk[14] – similar to the hand-glove model of enzymes – we will have a higher amount of active sites in larger particles, therefore reducing the activation energy for the phase transition.

Evolution of the ZIF-8 structure

In order to validate our analysis of the phase transition behaviour of ZIF-8 with different particle sizes, we performed *in situ* PXRD experiments for ZIF-8-98 and ZIF-8-0.14 upon the adsorption of N_2 at 80 K. Fig. 6a shows, as an example, the comparison of the PXRD patterns obtained for ZIF-8-0.14 before and after N_2 adsorption. During N_2 adsorption, all the peaks are shifted to lower angles, and the (004) (2θ = 11.11°) reflection shows a notable gain in intensity. Rietveld refinements to obtain crystallographic models were successful in both structures (Fig. S6†). Fig. 6b–d shows the rotation of the mIM rings and the bend of the methyl group from the planar

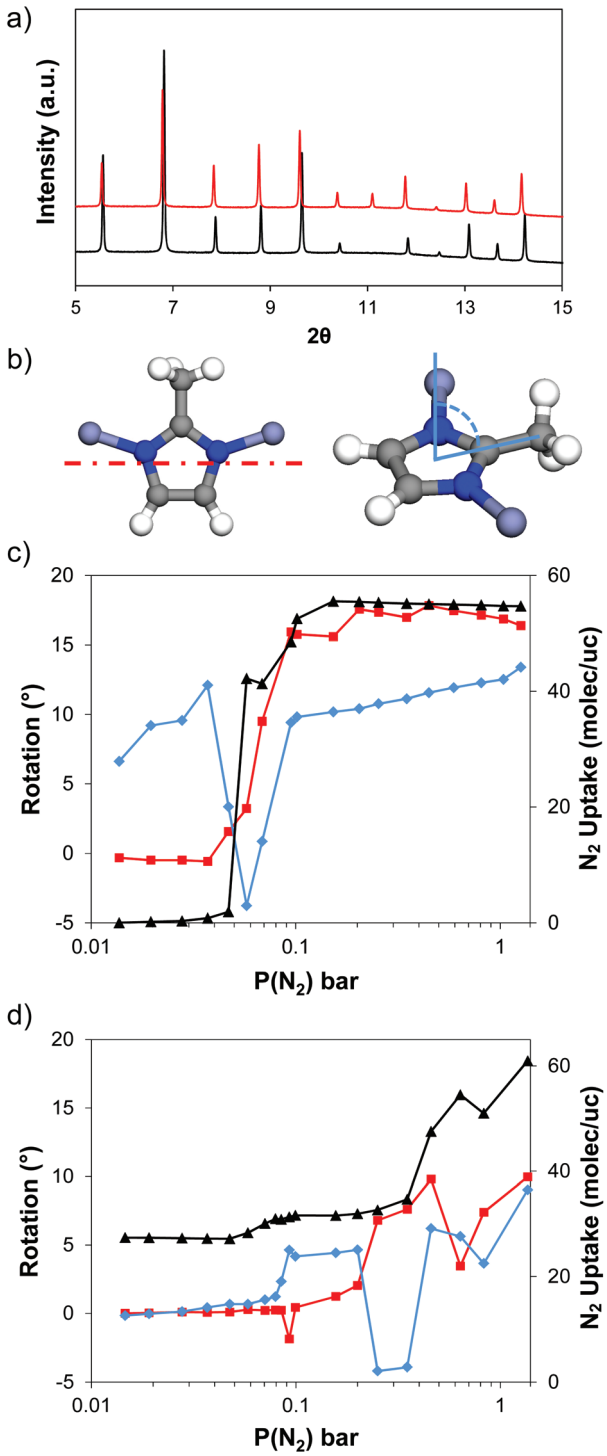

Fig. 6 (a) Comparison of PXRD patterns for ZIF-8-0.14 during *in situ* N_2 adsorption at 0 (black line) and 0.63 bar (red line). (b) Rotation of the mIM ring and methyl group respect to the mIM ring. Angle of rotation along with the amount of adsorbed N_2 molecules at different $p(N_2)$ for (c) ZIF-8-98 and (d) ZIF-8-0.14. Red square, rotation of mIM ring; blue diamond, bend of the methyl group; black triangle, N_2 uptake.

mIM rings with increasing adsorption pressure in both ZIF-8 samples, whereas Fig. S7† shows the changes in the *a* cell parameter. The N_2 uptakes measured during the *in situ* experiment

Open Access Article. Published on 26 February 2016. Downloaded on 20/04/2016 08:56:07.
This article is licensed under a Creative Commons Attribution 3.0 Unported Licence.

have been included in both figures as a reference. The amount adsorbed during the diffraction experiments differs from the equilibrium isotherms measured volumetrically; this difference is attributed to the fact that the gas adsorption during the *in situ* PXRD measurements is not fully equilibrated, and to the slightly higher adsorption temperature (80 *vs.* 77 K). Despite this, the two samples clearly present different trends during the *in situ* PXRD experiment: for ZIF-8-98 the uptake of gas is negligible below 0.05 bar; above this pressure the amount adsorbed increased up to 31 molecules per unit cell (220 cm^3 per g STP), followed by a second step up to *ca.* 55 molec per uc (390 cm^3 per g STP). In contrast, ZIF-8-0.14 started with a loading of 27 molec per uc (191 cm^3 per g STP) at low pressures and jumped up to *ca.* 31 molec per uc (220 cm^3 per g STP) at 0.07 bar, followed by a second step of *ca.* 54 molec per uc (380 cm^3 per g STP) at 0.6 bar.

Evolution of the structure in large particle size ZIF-8-98

Rietveld refinement of the activated ZIF-8 sample under vacuum and 80 K shows the well-known gate-closed ZIF-8AP structure,[13,41] with the methyl groups projecting into the pore windows and hindering the accessibility of N_2 molecules through the 4-ring windows. Upon adsorption of N_2 up to 0.0371 bar, the unit cell undergoes a slight decrease in volume by *ca.* 0.1% (~3.5 $Å^3$ for lattice parameter *a*). Over this range, the mIM ring configuration remained almost unaltered (Fig. 6). Interestingly, the methyl group bent from the mIM plane to open the window. Upon increasing the pressure to 0.0685 bar, the unit cell increases in volume by 0.8% (~41 $Å^3$), which is associated with a rotation of the mIM rings by up to 9° to open the pore windows, and a decrease in the degree of out-of-plane bending of the methyl group.

Fig. S8† shows the first adsorption site (observed from 0.0371 bar and 0.816 molec per uc), associated to Site I as described previously for adsorption of methane in ZIF-8.[14] At *ca.* 42 molec per uc (*i.e.* the first step at 0.0575–0.0685 bar), two additional N_2 adsorption sites in the centre of the 6-ring window (4.4 molec per uc) and the centre of the cavity (2.1 molec per uc) were identified, associated to Site II and Site III, respectively.[42] We termed this phase as the gate-closed large cell ZIF-8AP structure.

Interestingly, the PXRD patterns of ZIF-8-98 obtained at 0.0798 and 0.0868 bar showed a splitting of the diffraction peaks into three, indicating a mixture of different phases – probably due to the lack of equilibrium (Fig. S10†). These three phases were identified as: (i) the gate-closed ZIF-8AP structure (at $p(N_2)$ = 0 bar), (ii) the gate-closed large cell ZIF-8AP structure (observed at $p(N_2)$ = 0.0685 bar) and the (iii) gate-open ZIF-8HP structure ($p(N_2)$ > 0.0948 bar). Increasing adsorption pressure led to further N_2 uptake and the completion of the phase transition to ZIF-8HP structure. This was accompanied by an increase in unit cell volume by *ca.* 0.9% (~50 $Å^3$); after the phase transition, the unit cell volume remains approximately constant. At *ca.* 52 molec per uc (*i.e.* the second adsorption substep at pressures above 0.100 bar), the rotation of the mIM rings increased to 16°, whereas the methyl group bent between 9 and 12°. A new adsorption site was identified in the 4-ring window with 3.9 molec per uc adsorbed (Fig. S8c†), and was associated to Site IV.[14]

Evolution of the structure in small particle size ZIF-8-0.14

The evolution of ZIF-8-0.14 differed significantly from that of the ZIF-8-98. Under vacuum at 80 K, ZIF-8-0.14 adopts the gate-closed ZIF-8AP structure, although with a slightly smaller unit cell (ZIF-8-98, a = 17.00590(3) Å; ZIF-8-0.14, a = 16.98271(5) Å). At the lowest pressure measured (*i.e.* 0.0146 bar) three adsorption sites for N_2 molecules were identified in the structure (Fig. S9†), with 20.5 molec per uc, 3.5 molec per uc and 3.4 molec per uc adsorbed, respectively, giving a total of 27 N_2 molecules per unit cell. These sites correspond to Site I, II and III, respectively, as also identified in methane adsorption studies on ZIF-8.[14]

Increasing the adsorption pressure to 0.3500 bar led only to a small increase in the number of adsorbed molecules (*i.e.* 35 molec per uc). One additional adsorption site was observed at this pressure: Site IV 0.5 molec per uc at the centre of the 4-ring window. In this range of pressure, both the rotation of the mIM rings and the bend of the methyl groups increased gradually up to 7.6 and 3.9°, respectively. This was similar to the values obtained for the large crystal ZIF-8-98 and the intermediate step during the adsorption process. Increasing the adsorbate pressure led to a jump in the N_2 uptake, reaching 61 molec per uc at 1.3580 bar, as well as an increase in the rotation of the mIM rings and the bend of the methyl group up to 10 and 9°, respectively. This jump corresponds to the transition to the ZIF-8HP.

Overall, ZIF-8-0.14 showed a broader pressure range of transition compared with ZIF-8-98 (Fig. S6†). This is similar to the trend of phase transition in N_2 isotherms at 77 K. The overall rotation of the imidazole for ZIF-98 and ZIF-8-0.14 is 17° and 10°, respectively as shown in Fig. S11 and S12.†

Conclusions

We have studied the adsorption properties of a series of ZIF-8 materials with different particle sizes using high-resolution N_2 adsorption isotherms at 77 K and *in situ* PXRD. The pressure at which the gas-induced phase transition occurs (between ZIF-8AP and ZIF-8HP structures) is strongly influenced by the particle size of the ZIF-8 crystals. In this regard, small particle sizes of ZIF-8 (ZIF-8-0.14), showed a smoother and broader stepped adsorption behaviour as well as a hysteresis loop during desorption, compared with larger particle sizes (ZIF-8-98). These differences are caused by the higher energy barrier and smaller amount of active sites in the smaller particle size ZIF-8. The differences found during equilibrium adsorption are also extended to the adsorption kinetics. In this regard, more rigid ZIF-8-0.14 shows longer equilibration times than ZIF-8-98 at low pressures before the phase transition between ZIF-8AP and -HP. At higher pressures, when the ZIF-8 material adopts the ZIF-8HP structure,

 This journal is © The Royal Society of Chemistry 2016

Open Access Article. Published on 26 February 2016. Downloaded on 20/04/2016 08:56:07.
This article is licensed under a Creative Commons Attribution 3.0 Unported Licence.

equilibration times were significantly reduced and very similar between both ZIF-8-98 and ZIF-8-0.14. *In situ* PXRD studies during the adsorption of N_2 at 80 K showed changes in the rotation of both the 2-methylimidazole ring and the bend angle of the methyl group during the process. All these findings are of particularly importance in the design and engineering of new MOF adsorbents and MOF based mixed membranes, and to tune the selectivity properties of new materials for specific applications such as efficient CO_2 capture.[43]

Acknowledgements

This work was funded by the EPSRC IAA Partnership Development Award (RG/75759). D. F.-J. thanks the Royal Society for funding through a University Research Fellowship. We thank Diamond Light Source for beamtime at beamline I11 (visit EE9750).

Notes and references

1 K. S. Park, Z. Ni, A. P. Côté, J. Y. Choi, R. Huang, F. J. Uribe-Romo, H. K. Chae, M. O'Keeffe and O. M. Yaghi, *Proc. Natl. Acad. Sci. U. S. A.*, 2006, **103**, 10186.
2 P. Zhao, G. I. Lampronti, G. O. Lloyd, E. Suard and S. A. T. Redfern, *J. Mater. Chem. A*, 2014, **2**, 620.
3 H. Wu, W. Zhou and T. Yildirim, *J. Am. Chem. Soc.*, 2007, **129**, 5314.
4 A. Huang, Q. Liu, N. Wang and J. Caro, *Microporous Mesoporous Mater.*, 2014, **192**, 18.
5 J. Sanchez-Lainez, B. Zornoza, A. Mayoral, Á. Berenguer-Murcia, D. Cazorla-Amorós, C. Tellez and J. Coronas, *J. Mater. Chem. A*, 2015, **7**, 6549.
6 L. T. L. Nguyen, K. K. A. Le, H. X. Truong and N. T. S. Phan, *Catal. Sci. Technol.*, 2012, **2**, 521.
7 L. H. Wee, T. Lescouet, J. Ethiraj, F. Bonino, R. Vidruk, E. Garrier, D. Packet, S. Bordiga, D. Farrusseng, M. Herskowitz and J. A. Martens, *ChemCatChem*, 2013, **5**, 3562.
8 J. Cravillon, S. Münzer, S. J. Lohmeier, A. Feldhoff, K. Huber and M. Wiebcke, *Chem. Mater.*, 2009, **21**, 1410.
9 J. Cravillon, R. Nayuk, S. Springer, A. Feldho, K. Huber and M. Wiebcke, *Chem. Mater.*, 2011, 2130.
10 T. Tian, J. Velazquez-Garcia, T. D. Bennett and D. Fairen-Jimenez, *J. Mater. Chem. A*, 2015, **3**, 2999.
11 X.-C. Huang, Y.-Y. Lin, J.-P. Zhang and X.-M. Chen, *Angew. Chem., Int. Ed.*, 2006, **45**, 1557.
12 W. Zhou, H. Wu, M. R. Hartman and T. Yildirim, *J. Phys. Chem. C*, 2007, **111**, 16131.
13 D. Fairen-Jimenez, S. A. Moggach, M. T. Wharmby, P. A. Wright, S. Parsons and T. Düren, *J. Am. Chem. Soc.*, 2011, **133**, 8900.
14 D. Fairen-Jimenez, R. Galvelis, A. Torrisi, A. D. Gellan, M. T. Wharmby, P. A. Wright, C. Mellot-Draznieks and T. Düren, *Dalton Trans.*, 2012, **41**, 10752.
15 C. O. Ania, E. García-Pérez, M. Haro, J. J. Gutiérrez-Sevillano, T. Valdés-Solís, J. B. Parra and S. Calero, *J. Phys. Chem. Lett.*, 2012, **3**, 1159.
16 X. Zhang and J. Jiang, *J. Phys. Chem. C*, 2013, **117**, 18441.
17 H. Tanaka, S. Ohsaki, S. Hiraide, D. Yamamoto, S. Watanabe and M. T. Miyahara, *J. Phys. Chem. C*, 2014, **118**, 8445.
18 J.-P. Zhang, A.-X. Zhu and X.-M. Chen, *Chem. Commun.*, 2012, **48**, 11395.
19 G. Kumari, K. Jayaramulu, T. K. Maji and C. Narayana, *J. Phys. Chem. A*, 2013, **117**, 11006.
20 M. R. Ryder, B. Civalleri, T. D. Bennett, S. Henke, S. Rudić, G. Cinque, F. Fernandez-Alonso and J.-C. Tan, *Phys. Rev. Lett.*, 2014, **113**, 215502.
21 N. Y. Tan, M. T. Ruggiero, C. Orellana-Tavra, T. Tian, A. D. Bond, T. M. Korter, D. Fairen-Jimenez and J. A. Zeitler, *Chem. Commun.*, 2015, **51**, 16037.
22 M. E. Casco, Y. Cheng, L. Daeman, D. Fairen-Jimenez, E. V. Ramos-Fernández, A. J. Ramirez-Cuesta and J. Silvestre-Albero, *Chem. Commun.*, 2016, **52**, 3639.
23 C. Zhang, J. A. Gee, D. S. Sholl and R. P. Lively, *J. Phys. Chem. C*, 2014, **118**, 20727.
24 F.-X. Coudert, *Phys. Chem. Chem. Phys.*, 2010, **12**, 10904.
25 S. R. Venna, J. B. Jasinski and M. A. Carreon, *J. Am. Chem. Soc.*, 2010, **132**, 18030.
26 E. Haldoupis, T. Watanabe, S. Nair and D. S. Sholl, *ChemPhysChem*, 2012, **13**, 3449.
27 H. Bux, F. Liang, Y. Li, J. Cravillon and M. Wiebcke, *J. Am. Chem. Soc.*, 2009, **131**, 16000.
28 Y. Pan, Y. Liu, G. Zeng, L. Zhao and Z. Lai, *Chem. Commun.*, 2011, **47**, 2071.
29 K. Kida, M. Okita, K. Fujita, S. Tanaka and Y. Miyake, *CrystEngComm*, 2013, **15**, 1794.
30 C. Zhang, R. P. Lively, K. Zhang, J. R. Johnson, O. Karvan and W. J. Koros, *J. Phys. Chem. Lett.*, 2012, **3**, 2130.
31 S. P. Thompson, J. E. Parker, J. Potter, T. P. Hill, A. Birt, T. M. Cobb, F. Yuan and C. C. Tang, *Rev. Sci. Instrum.*, 2009, **80**, 075107.
32 S. P. Thompson, J. E. Parker, S. J. Day, A. Evans and C. C. Tang, *Eur. Astron. Soc. Publ. Ser.*, 2012, **58**, 225.
33 J. E. Parker, J. Potter, S. P. Thompson, A. R. Lennie and C. C. Tang, *Mater. Sci. Forum*, 2012, **706–709**, 1707.
34 A. Coelho, *TOPAS-Academic v5*, Coehlo Software, Brisbane, Australia, 2012.
35 G. W. Stinton and J. S. O. Evans, *J. Appl. Crystallogr.*, 2007, **40**, 87.
36 M. C. McCarthy, V. Varela-Guerrero, G. V. Barnett and H. K. Jeong, *Langmuir*, 2010, **26**, 14636.
37 J. Rouquerol, F. Rouquerol, K. S. W. Sing, P. Llewellyn, G. Maurin and K. S. W. Sing, *Adsorption by powders and porous solids*, 2014.
38 D. Fairen-Jimenez, N. A. Seaton and T. Düren, *Langmuir*, 2010, **26**, 14694.

39 S. Watanabe, H. Sugiyama, H. Adachi, H. Tanaka and M. T. Miyahara, *J. Chem. Phys.*, 2009, **130**, 164707.
40 Y. Sakata, S. Furukawa, M. Kondo, K. Hirai, N. Horike, Y. Takashima, H. Uehara, N. Louvain, M. Meilikhov, T. Tsuruoka, S. Isoda, W. Kosaka, O. Sakata and S. Kitagawa, *Science*, 2013, **193**, 193.
41 S. A. Moggach, T. D. Bennett and A. K. Cheetham, *Angew. Chem., Int. Ed.*, 2009, **48**, 7087.
42 H. Wu, W. Zhou and T. Yildirim, *J. Phys. Chem. C*, 2009, **113**, 3029.
43 B. Seoane, J. Coronas, I. Gascon, M. E. Benavides, O. Karvan, J. Caro, F. Kapteijn and J. Gascon, *Chem. Soc. Rev.*, 2015, **44**, 2421.

Open Access Article. Published on 26 February 2016. Downloaded on 20/04/2016 08:56:07.
This article is licensed under a Creative Commons Attribution 3.0 Unported Licence.

This journal is © The Royal Society of Chemistry 2016

Electronic Supplementary Material (ESI) for Dalton Transactions.
This journal is © The Royal Society of Chemistry 2016

Electronic Supporting Information for:

Role of Crystal Size on Swing-Effect and Adsorption Induced Structure Transition of ZIF-8

Tian Tian,[a] Michael T. Wharmby,[b] José B. Parra,[c] Conchi O. Ania[c] and David Fairen-Jimenez[a,*]

[a]*Department of Chemical Engineering & Biotechnology, University of Cambridge, Pembroke Street, Cambridge CB2 3RA, United Kingdom. Email: df334@cam.ac.uk; website: http://people.ds.cam.ac.uk/df334*

[b]*Diamond Light Source Ltd., Diamond House, Harwell Science & Innovation Campus, Didcot, Oxon., OX11 0DE UK*

[c]*Instituto Nacional del Carbón, INCAR-CSIC, Oviedo, Spain*

Contents

S1 Instruments

X-ray diffraction (XRD) patterns were recorded with a Bruker D8 diffractometer using CuKα_1 (λ=0.15405 Å^{-1}) radiation with a step of 0.02° at a scanning speed of 0.1°s^{-1}. Scanning electron microscope (SEM) images were taken by Hitachi S-5500 FE SEM with an accelerating voltage of 5kV without gold coating. N_2 adsorption isotherms were undertaken at 77 K using a Micromeritics ASAP 2020 instrument. Prior to the N_2 adsorption, all samples were evacuated overnight for 24 h at 423 K under vacuum.

S2 Particle size distribution

For each sample, 100 particles were randomly selected to measure the size by using Hitachi S-5500 FE SEM. The size distribution, together with average size and standard deviation (SD) are shown in Figure S1.

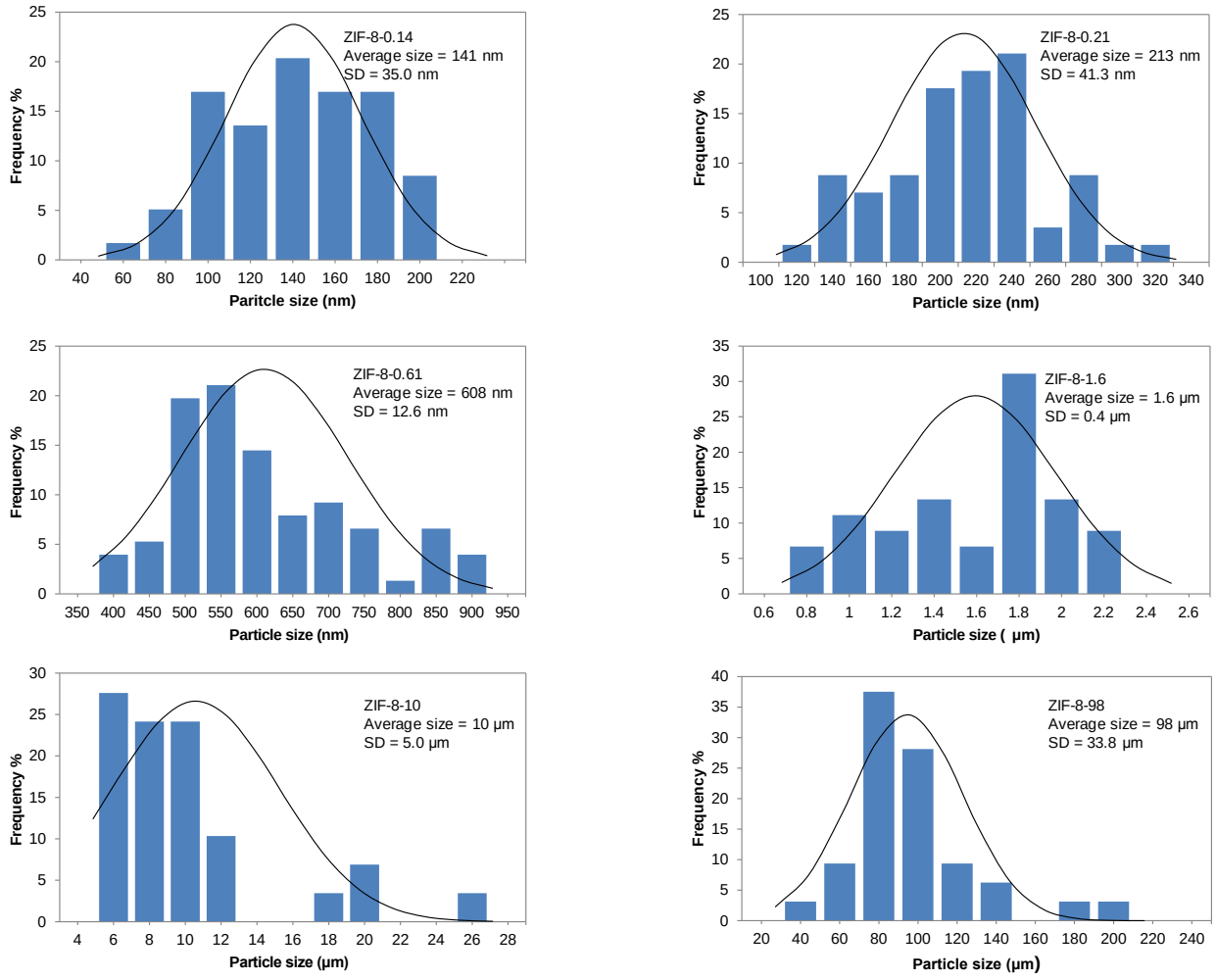

Fig. S1. Size distribution and normal distribution of different ZIF-8 samples.

S3 BET representation

BET area was calculated by Rouquerol's consistency criteria.[1] The plot on left in Fig S2 was used to select the maximum P/P_0 for calculation. The plot on right in Fig S2 was the BET representation by using selected P/P_0. The plot was not linear due to the phase transition.

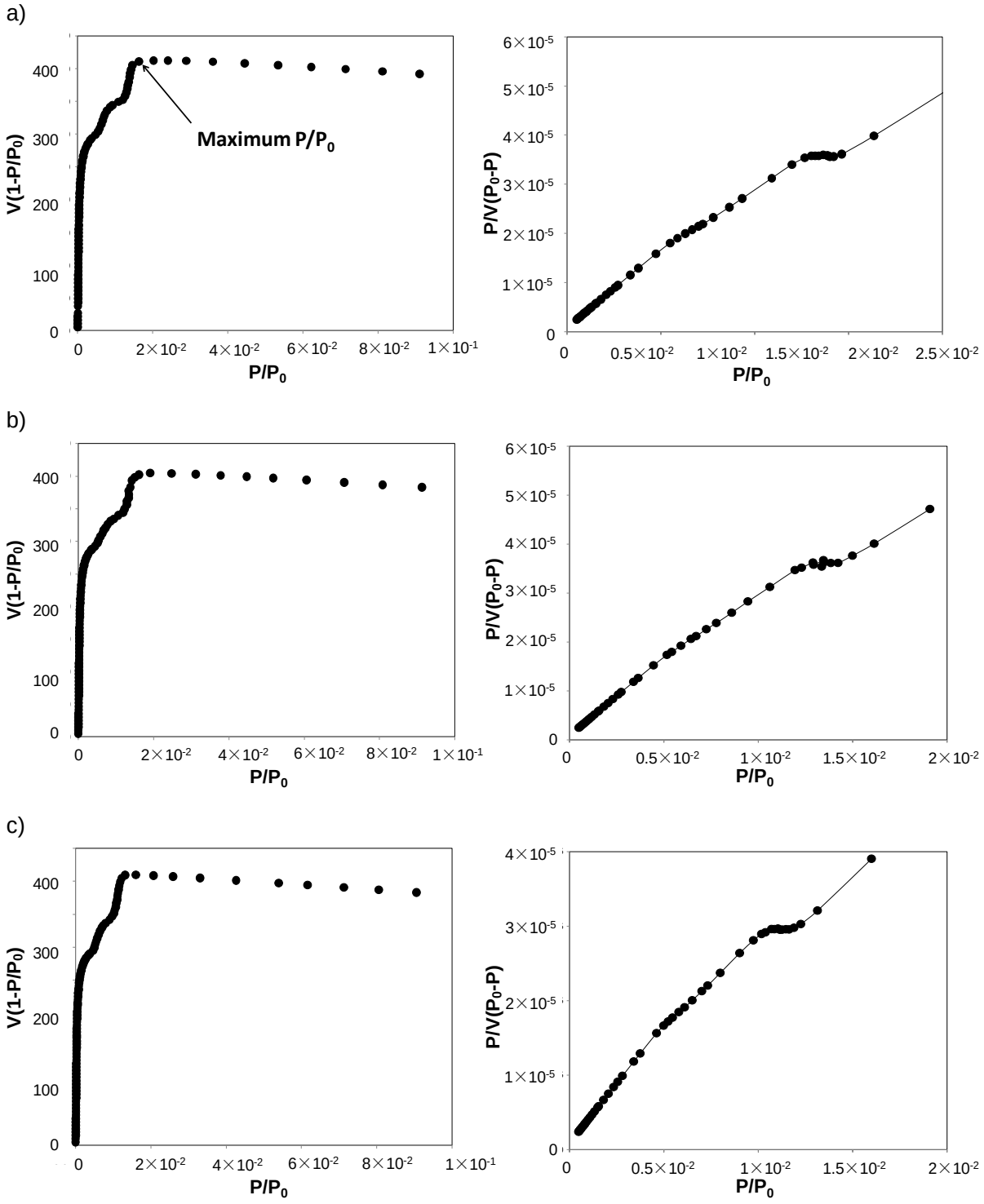

Fig. S2a. Plot to determine maximum P/P_0 by applying Rouquerol's consistency criteria ***(left)*** and BET representation of N_2 isotherms ***(right).*** **a)** ZIF-8-0.14, **b)** ZIF-8-0.21, **c)** ZIF-8-0.61.

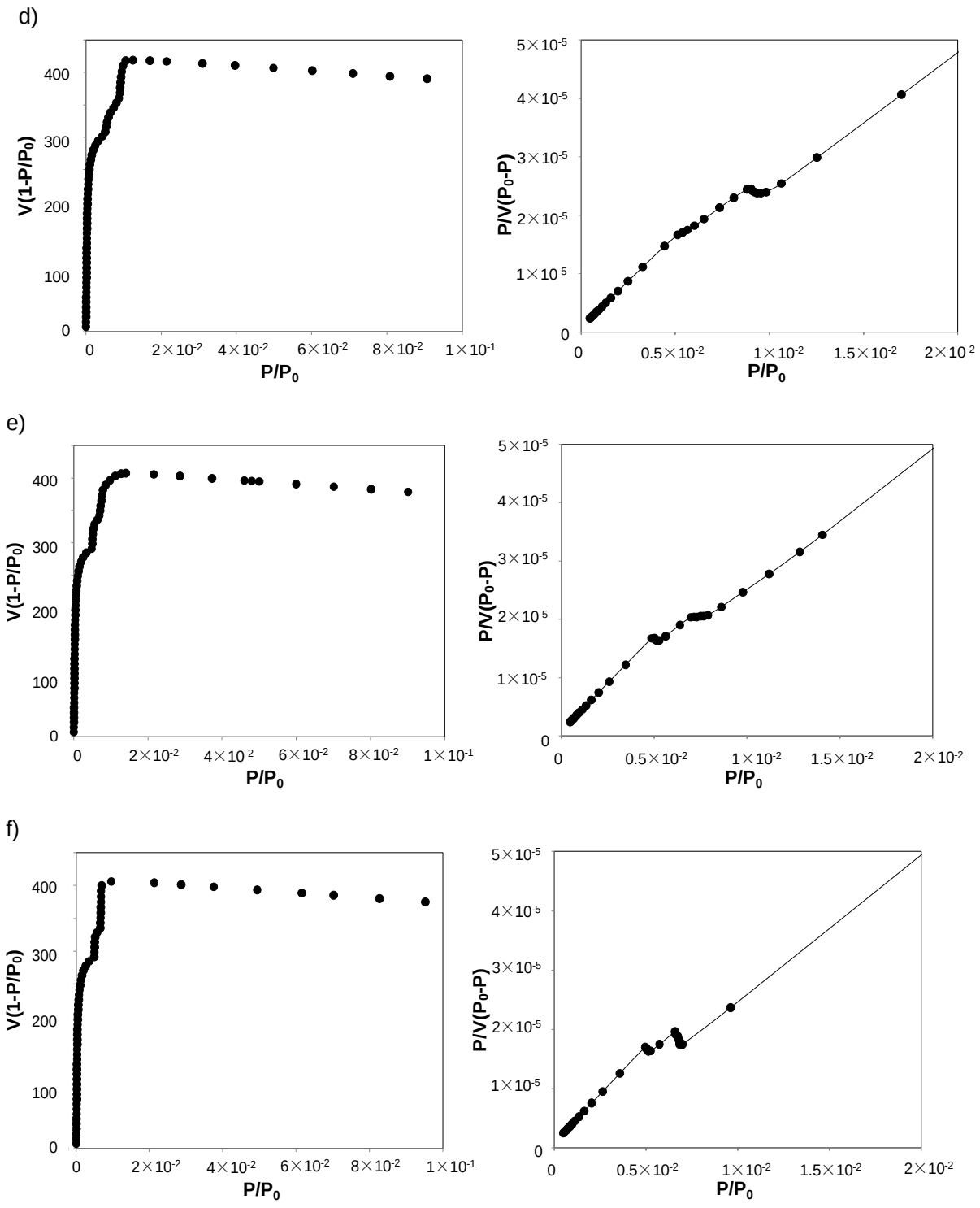

Fig. S2b. Plot to determine maximum P/P_0 by applying Rouquerol's consistency criteria ***(left)*** and BET representation of N_2 isotherms ***(right)*.** **d)** ZIF-8-1.6, **e)** ZIF-8-10, **f)** ZIF-8-98.

S4 N_2 adsorption/desorption

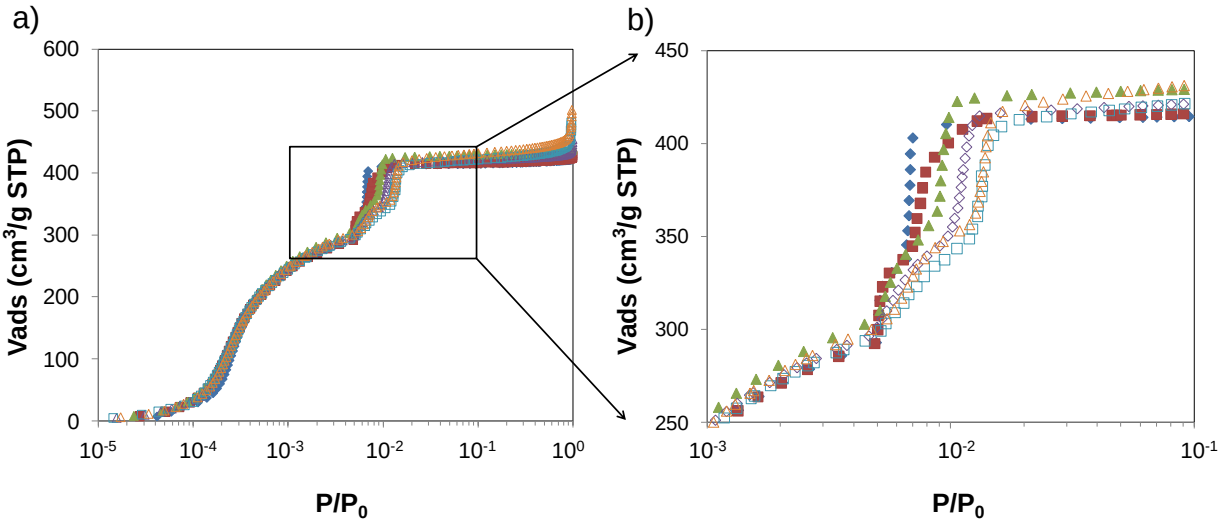

Fig. S3. a) Semi-log plot of N_2 adsorption isotherms at 77 K in ZIF-8 samples with different particle size. Blue closed diamonds, ZIF-98; red closed squares, ZIF-8-10; green closed triangles, ZIF-8-1.6; purple open diamonds, ZIF-8-0.61; blue open squares, ZIF-8-0.21; orange open triangles, ZIF-8-0.14. **b)** Detail of the N_2 adsorption isotherms plot in the phase transition region.

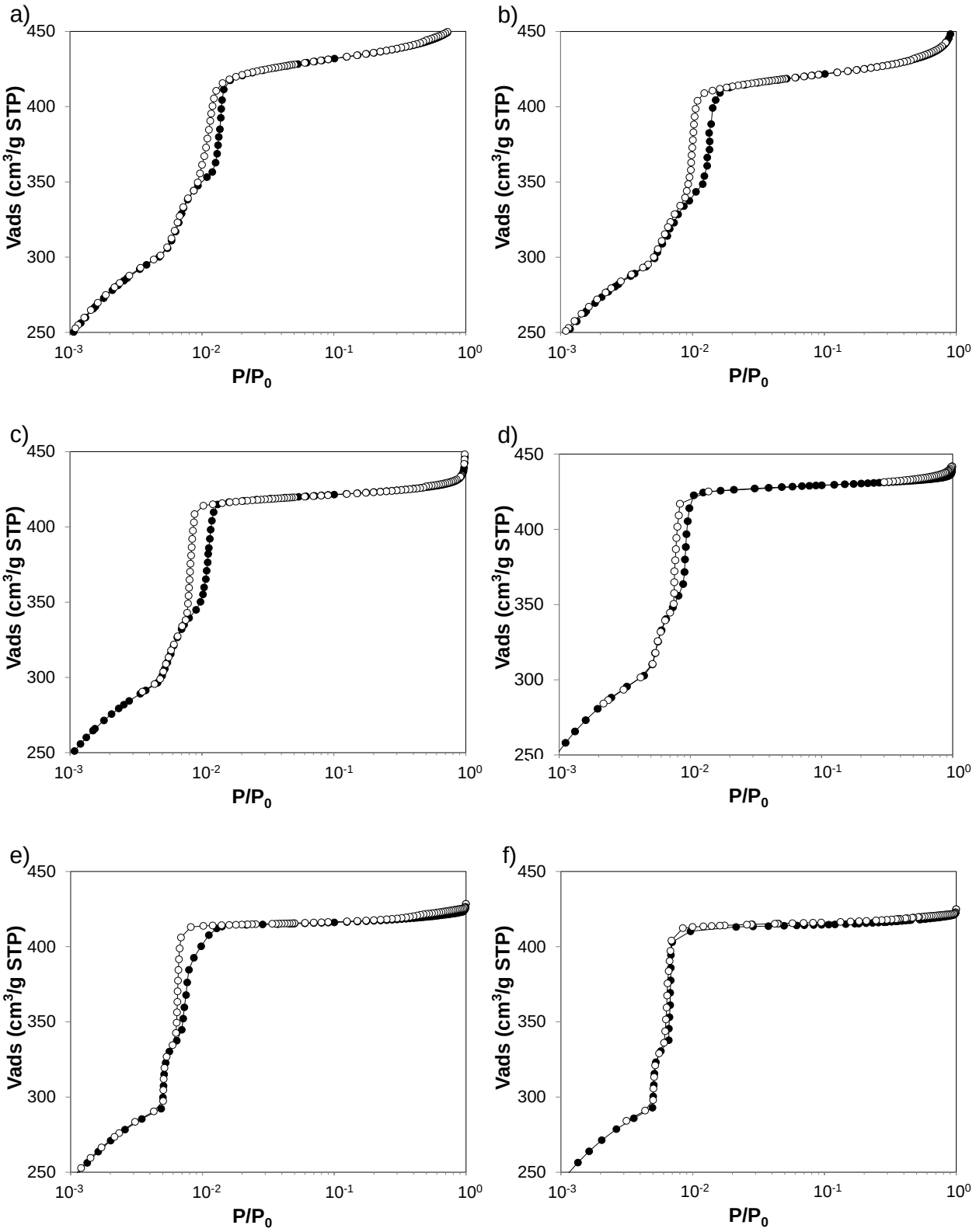

Fig. S4. N_2 adsorption and desorption of ZIF-8 with different particle sizes. **a)** ZIF-8-0.14, **b)** ZIF-8-0.21, **c)** ZIF-8-0.61, **d)** ZIF-8-1.6, **e)** ZIF-8-10, **f)** ZIF-8-98. Closed circles, adsorption; open circles, desorption.

S5 Equilibrium time

The adsorption/desorption equilibrium time for all samples was shown in Fig S5. Before the structure opening, the adsorption time was different for different samples due to the different flexibility of the structure, which highly affects the diffusion of the molecules. The adsorption time was significantly increased at the onset pressure for the two stepped adsorption process. This is mainly due to the rearrangement of adsorbed gas and filling of new gas molecules at the 4-ring window. After the structure transition, the equilibrium time was declined due to the easy accessibility for the opened structure. The same trend was observed for desorption process. The equilibrium time was increased at the threshold pressure for hysteresis loop due to the structure transition and rearrangement of the remaining gases.[2]

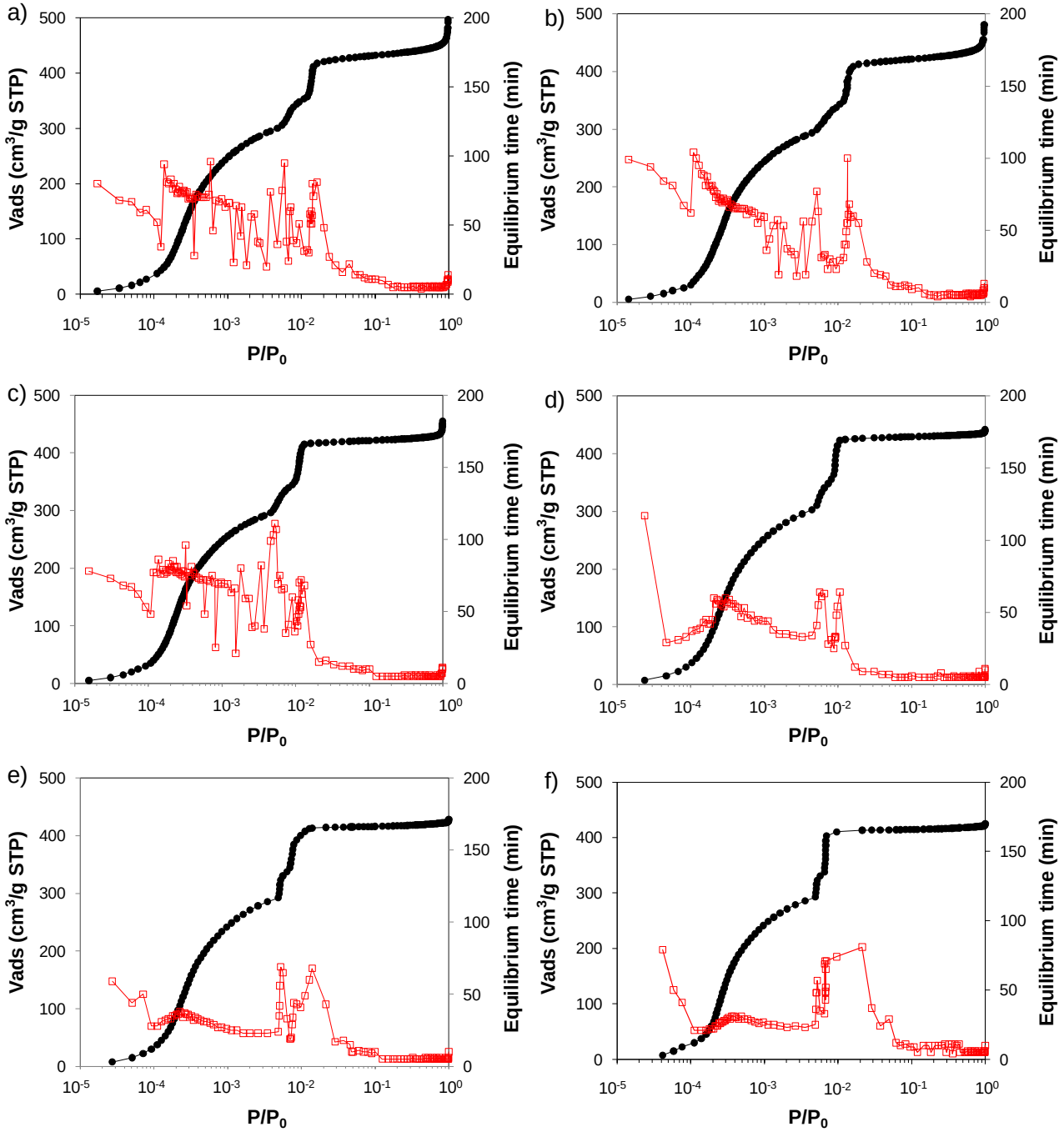

Fig. S5. N_2 adsorption along with equilibrium time for **a)** ZIF-8-0.14, **b)** ZIF-8-0.21, **c)** ZIF-8-0.61, **d)** ZIF-8-1.6, **e)** ZIF-8-10, **f)** ZIF-8-98. Black closed circle, adsorption; red open square, adsorption equilibrium time.

S6 *In situ* XRD

Sample Preparation

ZIF-8-0.14

ZIF-8-0.14, already in the form of a fine powder, was ground in a pestle and mortar to ensure the sample was fully homogenous. The powder was then loaded into a 0.5 mm quartz glass capillary and secured in place by packing a small ball of class wool on top of the powder. The capillary was then inserted into a brass sealing stub and sealed in place with epoxy resin. Finally the funnel end of the capillary was snapped off and the whole assembly was secured by a Swagelok® fitting in to the I11 gas cell.[3,4]

ZIF-8-98

ZIF-8-98 was obtained as large blocky and intergrown crystals. The sample was very gently and briefly ground, to yield a particle size that could be loaded into a capillary. As for the ZIF-8-0.14, the powder was loaded into a 0.5 mm quartz glass capillary and secured in place with a small ball of glass wool. It should be noted that due to the large particle size the packing was significantly less homogenous than normally desirable, however this was necessary to facilitate investigation of the particle size effect on structural responsiveness. After loading, the capillary was inserted into a brass sealing stub and sealed in place with epoxy resin. Finally the funnel end of the capillary was snapped off and the whole assembly was secured by a Swagelok® fitting in to the I11 gas cell.[3,4]

Data Collection Details

All diffraction patterns in this work were collected using the in-house developed 90° arc position sensitive detector at beamline I11,[5] collecting 8 partial patterns each at a different δ angle (range δ = 2.0°-3.75°; step size of 0.25°) for 1 sec. Patterns were then summed together to remove the gaps between detector plates. Whilst collecting data, the sample was repeatedly rocked on the θ circle through 30° to provide some powder averaging.

Activation

Both ZIF-8-0.14 and ZIF-8-98 were activated in the same way, first offline for about an hour prior to mounting on the diffractometer using a tube furnace heated to 413 K and under dynamic vacuum provided by a turbomolecular pump ($p \sim 1\times10^{-6}$ mbar). The sample was then transferred to the diffractometer on beamline I11 at Diamond Light Source (Oxon., UK)[6] and a diffraction pattern was collected. The sample was activated again for a further 20 mins using an Oxford cryostream heated to 413 K and the turbomolecular pump of the I11 gas handling system.[3,4] A second diffraction pattern was collected after activation to check the degree of sample degradation, before the sample was cooled under dynamic vacuum to 80 K, using the cryostream.

In Situ Experiment

Once cooled to 80 K, a diffraction pattern of each sample was collected at a pressure of 0 bar (measured using the I11 gas handling system). N_2 gas was then dosed onto the sample, using the I11 gas handling system. A series of 12 pressure points, approximately equally spaced over the range $p(N_2)$ = 0.00-0.10 bar (p/p_0 = 0.00-0.07; p_0 taken as 1.3687 at 80 K)[7] were then collected (Table S1). A second series 10 of points were collected with wider spacing over the range $p(N_2)$ = 0.10-1.35 (p/p_0 = 0.07-0.99) (Table S1). At each

pressure point, the N_2 pressure in the sample was allowed to equilibrate for 10 mins and the rate of change of the pressure was then observed. If the rate of change was greater than 0.1 mbar in 20 secs, the sample was allowed to equilibrate for a further 5 mins and the rate of change checked again; this process was repeated until the N_2 pressure stabilised. A diffraction pattern of the sample was then collected using the PSD, as described for the activation procedure.

Table S1. N_2 adsorbate pressures at which diffraction patterns were collected for ZIF-8-0.14 and ZIF-8-98 during the *in situ* adsorption experiment.

ZIF-8-0.14/ bar	ZIF-8-98 / bar
0.0000	0.0000
0.0146	0.0069
0.0191	0.0137
0.0277	0.0196
0.0368	0.0278
0.0474	0.0371
0.0581	0.0469
0.0705	0.0575
0.0794	0.0685
0.0847	0.0798
0.0927	0.0868
0.0994	0.0948
0.1566	0.1015
0.2001	0.1526
0.2506	0.2044
0.3500	0.2544
0.4576	0.3486
0.6364	0.4481
0.8284	0.5921
1.0020	0.8079
1.2473	1.0367
1.3580	1.2612
	1.3486

Data Analysis

Each data set was reprocessed to a data range of 2.0°-55.0° with a bin size of 0.004° 2θ using a bespoke Python script. All indexing, Pawley fitting and Rietveld refinement operations, including parametric Rietveld refinement, were performed using the routines implemented in the TOPAS-Academic v5 suite.[8] It was possible to index all of the diffraction patterns in this work in the reported cubic space group for ZIF-8, $I4\bar{3}m$.

Initial Rietveld Refinements

The diffraction patterns measured for both samples under vacuum were indexed and Pawley fitted. A Rietveld refinement was then performed, using the background, peak profile and unit cell parameters

determined from the Pawley fit, along with the previously reported activated ZIF-8 structure,[9,10] as a starting model. To account for the poorer averaging of the ZIF-8-98, additional preferred orientation (spherical harmonic model) terms were included in the refinement. To ensure a chemically sensible result, restraints were applied to the Zn-N, N-C and C-C distances, as well as N···C, C···C and N···N non-bonding distances. A further restraint was applied to ensure the imidazolate ring remained flat. The same set of restraints was used for all Rietveld refinements, including the parametric refinement, and these are summarised in Table S2. Good fits to both sets of data were achieved and refinement quality indicators along with the final refined unit cells are included in Table S3.

Table S2. Restraints applied to the framework during the Rietveld refinement, with a schematic of the imidazolate linker and one Zn atom to show where these restraints are applied.

Restraint	Distance ± Tolerance / Å
Zn-N	1.99 ± 0.001
C1-C1	1.37 ± 0.001
C1-N1	1.37 ± 0.001
N1-C2	1.30 ± 0.001
C2-C3	1.52 ± 0.001
C1…N1a	2.37 ± 0.005
C1…C2	2.31 ± 0.005
N1…N1a	2.25 ± 0.005
C1, N1, C2, C3 (Dihedral angle)	0.0° ± 0.001°

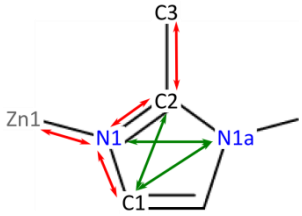

In the next stage, diffraction pattern measured at the maximum N_2 pressures for each sample (ZIF-8-0.14: $p(N_2)$ = 1.3580 bar, p/p_0 = 0.992; ZIF-8-98: $p(N_2)$ = 1.3486 bar, p/p_0 = 0.985) were analysed. Data were indexed and Pawley fits were performed and the profile and cell parameters from these used as starting points for the Rietveld refinement. The respective structure under vacuum was used as a starting point for the refinement, with the restraint set described applied. The positions of the imidazolate linker were then allowed to refine. Once this stabilised, a Fourier difference map was calculated and on the most likely (highest peak) positions, a N_2 molecule was placed. Each N_2 molecule was described as a rigid body, with two N atoms separated by a distance of 1.098 Å; the position of the molecule was described with a 'fake' atom referred to as the Centre Of Mass (COM), placed half way between the two N atoms. Occupancies and orientation of the each molecule were refined first, followed by the position. If molecule's occupancy tended to 0, it was removed and an alternative Fourier difference peak was chosen as an N_2 molecule. By this sequential process a model of the structure of the adsorbed N_2 molecules was developed. In the final cycles of refinement, occupancy and orientation of the N_2 molecules was fixed and the positions and displacement parameters of the N_2 adsorbates and framework were refined together. Good fits to the data were again obtained and the refinement quality indicators are included in Table S3.

Rietveld Refinements at Intermediate Pressures

To identify structural changes in the samples occurring at intermediate N_2 pressures, diffraction patterns were initially visually inspected for obvious shifts in peak positions. For ZIF-8-0.14, four phases with peaks not consistent with either the evacuated or $p(N_2)$ = 1.3580 bar structures were identified, whilst for ZIF-8-98 only three phases were identified. However, it was found that diffraction patterns of ZIF-8-98 measured at $p(N_2)$ = 0.0798 and 0.0868 bar contained peaks attributed to either two or three of the other observed phases. Thus, these measurements were discarded in subsequent analysis steps.

Each identified phase was Rietveld refined separately, using the structure nearest in N_2 pressure as a starting point. The framework of each structure was refined using the restraints listed in Table S2 and the

structure of the adsorbates was determined using the method described for the p/p_0~1 structures. In the final cycles of refinement, the framework and adsorbate structures were refined together; the final refinement quality indicators are given in Table S3.

Table S3. List of refinement quality parameters and lattice parameters obtained from the final Rietveld refinements of ZIF-8-0.14 and ZIF-8-98 determined as a function of N_2 adsorbate pressure.

ZIF-8-0.14

N_2 Pressure (p/p_0) / bar (-)	Cell Parameter / Å	R_{wp} / %	R_{Bragg} / %	χ^2
0.0000 (0.000)	16.98205(8)	1.84	2.36	6.708
0.0847 (0.062)	17.03920(10)	2.54	2.34	12.302
0.0927 (0.068)	17.03985(8)	1.68	1.22	5.400
0.4576 (0.334)	17.04902(8)	1.60	1.03	4.858
0.6364 (0.465)	17.06286(7)	1.82	1.17	6.311
1.3580 (0.992)	17.10080(7)	1.62	1.24	5.020

ZIF-8-98

N_2 Pressure (p/p_0) / bar (-)	Cell Parameter / Å	R_{wp} / %	R_{Bragg} / %	χ^2
0.0000 (0.000)	17.00499(6)	5.24	5.03	41.967
0.0371 (0.027)	17.00076(5)	4.09	3.02	26.051
0.0575 (0.042)	17.05138(7)	4.87	5.72	36.244
0.0948 (0.069)	17.11474(6)	4.19	3.53	26.788
1.3486 (0.985)	17.11853(3)	3.13	1.94	15.194

Parametric Rietveld Refinement

The individually refined structures were used to set up a parametric Rietveld refinement; during this refinement, the unit cell parameters and atomic positions of these structures were fixed. Initial models of the structures at pressure between the refined structures were derived from the refined structure bounding the range with the highest pressure (e.g. for ZIF-8-0.14 structures between 0.0146 and 0.0794 bar, the 0.0847 bar structure was used rather than the 0.0000 bar structure). Peak profile, background and displacement parameters were constant across all structures. Lattice parameters of the all the unrefined phases were allowed to refine freely. Framework structure was alternately refined with N_2 molecule orientation and occupancy until the refinement was relatively stable, at which point all were refined together. N_2 molecule occupancy was restrained to be greater than the previous structure's occupancy whilst lower than the subsequent structure's, assuming that as the N_2 pressure increases, so the adsorbed amount also increases. Only in the last cycles of refinement were the thermal parameters also refined. Good fits to the data were obtained for the final cycles of both structures – fit quality indicators, and unit cell parameters from the parametric Rietveld refinement are given in Table S4.

Table S4. Results of parametric Rietveld refinement: fit quality indicators and lattice parameters as a function of pressure.

ZIF-8-0.14

N_2 Pressure (p/p_0) / bar (-)	Cell Parameter / Å	R_{wp} / %	R_{Bragg} / %	χ^2
0.0000 (0.000)	16.98289(4)	2.16	3.13	9.276
0.0146 (0.011)	16.99929(4)	2.06	2.09	8.155
0.0191 (0.014)	16.99929(4)	1.90	1.77	6.884
0.0277 (0.020)	16.99929(4)	1.84	1.59	6.495
0.0368 (0.027)	16.99934(4)	1.80	1.52	6.240
0.0474 (0.035)	17.00051(4)	1.80	1.55	6.254
0.0581 (0.042)	17.00676(4)	1.81	1.62	6.239
0.0705 (0.052)	17.01928(4)	1.78	1.53	6.114
0.0794 (0.058)	17.03359(4)	1.84	1.75	6.436
0.0847 (0.062)	17.03847(4)	1.97	2.24	7.368
0.0927 (0.068)	17.03994(4)	1.80	1.16	6.178
0.0994 (0.073)	17.04100(4)	1.85	1.37	6.502
0.1566 (0.114)	17.03950(4)	2.03	2.07	7.775
0.2001 (0.146)	17.03853(4)	2.23	2.51	9.458
0.2506 (0.183)	17.03873(4)	2.57	3.34	12.440
0.3500 (0.256)	17.04065(4)	2.88	3.68	15.773
0.4576 (0.334)	17.04969(4)	2.35	3.32	10.449
0.6364 (0.465)	17.06290(5)	1.97	1.87	7.342
0.8284 (0.605)	17.07699(4)	2.03	1.70	7.813
1.0020 (0.732)	17.08662(4)	1.92	1.67	7.026
1.2473 (0.911)	17.09597(4)	2.05	2.06	7.980
1.3580 (0.992)	17.10034(4)	2.34	3.35	10.425

ZIF-8-98

N_2 Pressure (p/p_0) / bar (-)	Cell Parameter / Å	R_{wp} / %	R_{Bragg} / %	χ^2
0.0000 (0.000)	17.00590(3)	5.52	4.94	46.646
0.0069 (0.005)	17.00492(3)	4.97	7.71	38.502
0.0137 (0.010)	17.00381(3)	3.49	2.83	18.979
0.0196 (0.014)	17.00278(3)	3.61	3.07	20.241
0.0278 (0.020)	17.00229(3)	3.71	3.58	21.777
0.0371 (0.027)	17.00185(3)	4.38	3.59	30.3007
0.0469 (0.034)	17.00507(4)	8.86	7.46	121.668
0.0575 (0.042)	17.05243(3)	4.91	5.61	36.848
0.0685 (0.050)	17.05734(3)	8.61	15.79	114.358
0.0798 (0.058)				
0.0868 (0.063)				
0.0948 (0.069)	17.11437(3)	4.67	5.06	33.355
0.1015 (0.074)	17.11421(3)	3.92	4.16	23.588
0.1526 (0.111)	17.11555(3)	5.03	5.54	38.729
0.2044 (0.149)	17.11558(3)	4.18	3.52	26.982
0.2544 (0.186)	17.11613(3)	3.41	3.66	17.973
0.3486 (0.255)	17.11677(3)	3.62	3.16	20.368
0.4481 (0.327)	17.11731(3)	4.27	3.43	28.233
0.5921 (0.433)	17.11784(3)	3.52	3.53	19.011
0.8079 (0.590)	17.11857(3)	3.49	3.91	19.075
1.0367 (0.757)	17.11895(3)	3.35	2.96	17.386
1.2612 (0.921)	17.11889(3)	3.88	5.39	23.497
1.3486 (0.985)	17.11918(3)	3.53	3.05	19.360

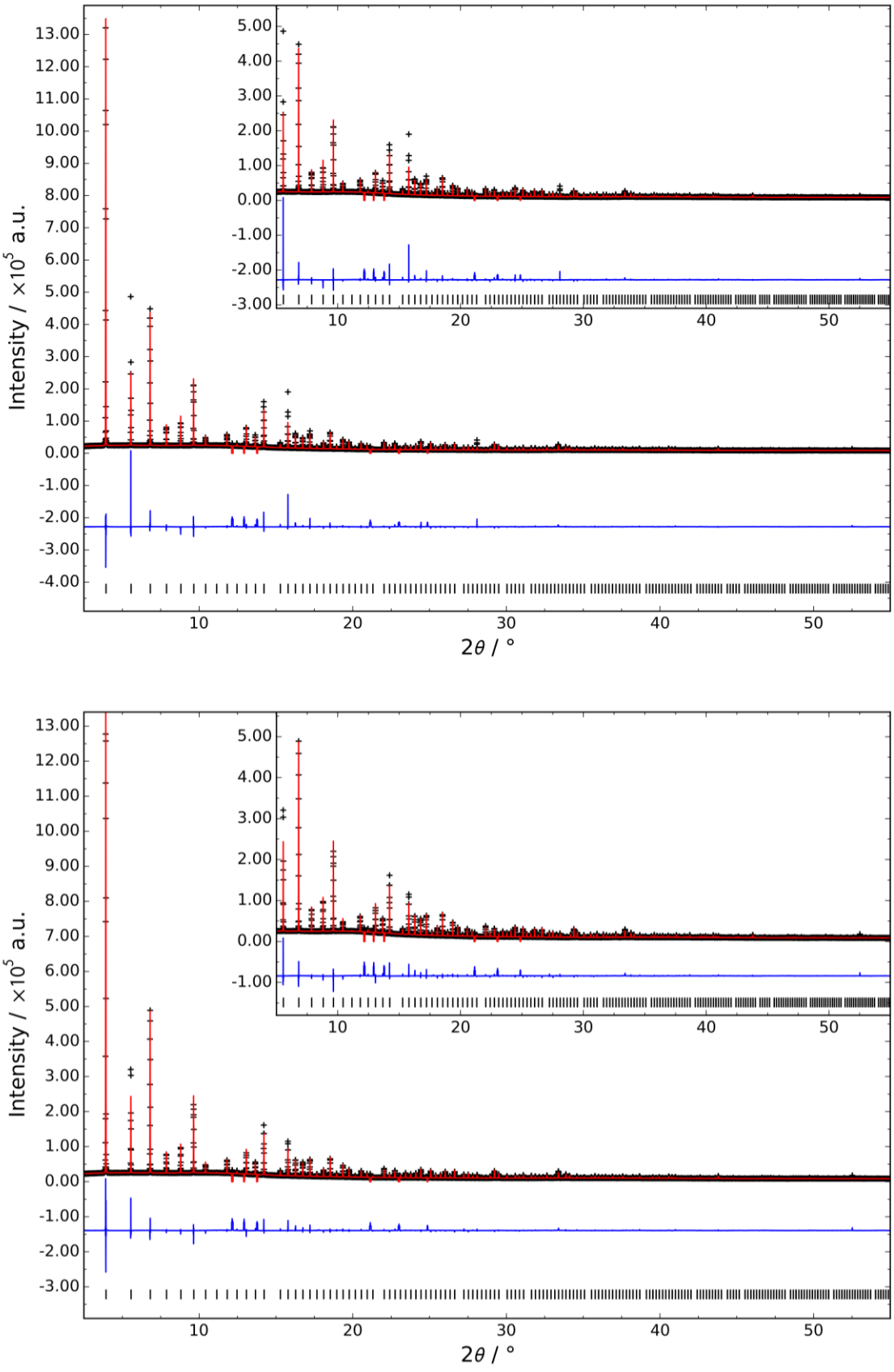

Figure S6a. Observed (black), refined (red), and difference (blue) X-Ray diffraction profiles measured for **(top)** empty ZIF-8-98, and **(bottom)** ZIF-8-98 loaded with N_2 at 0.0371 bar.

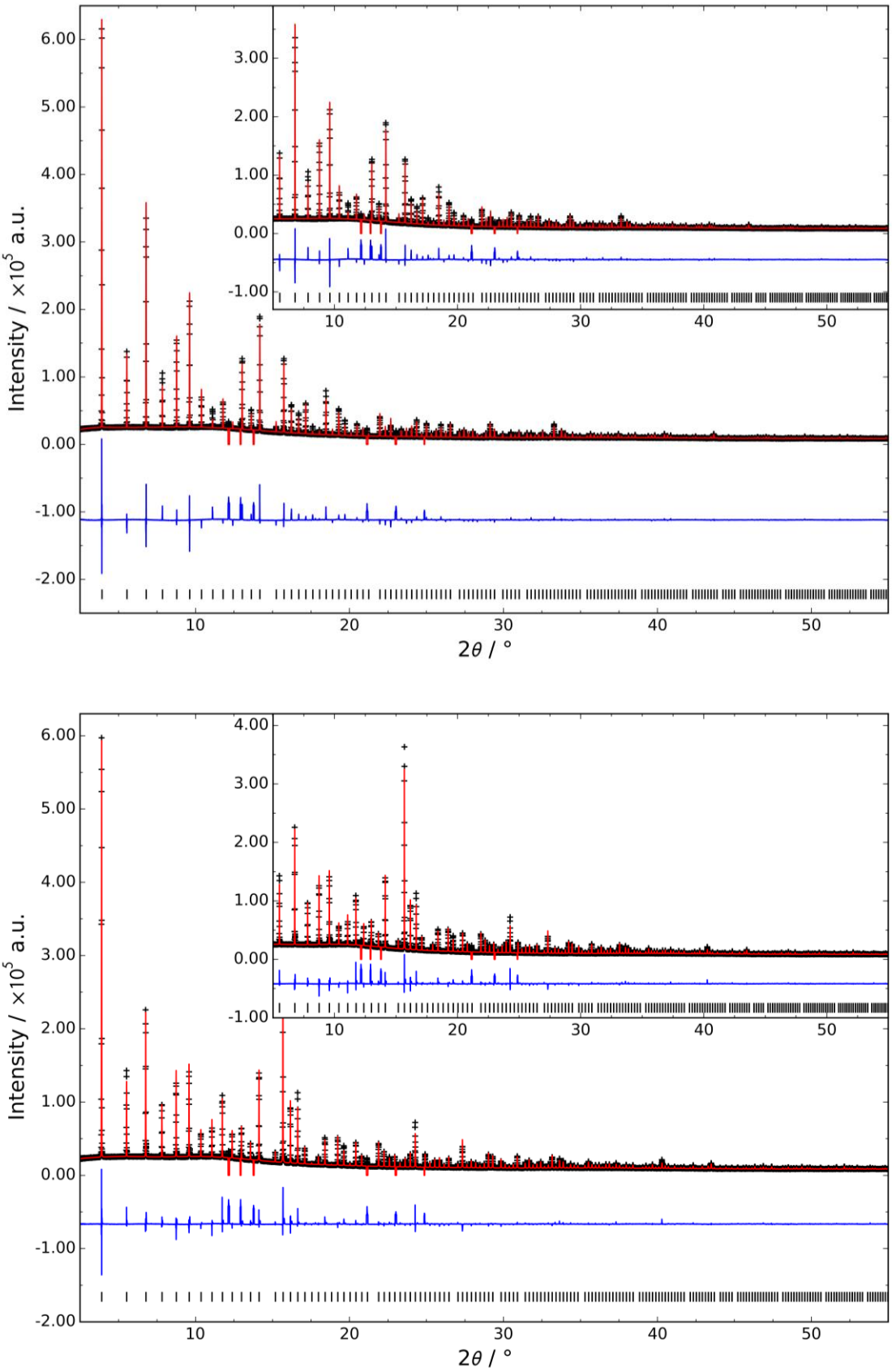

Figure S6b. Observed (black), refined (red), and difference (blue) X-Ray diffraction profiles measured for **(top)** ZIF-8-98 loaded with N_2 at 0.0575 bar, and **(bottom)** ZIF-8-98 loaded with N_2 at 0.0948 bar.

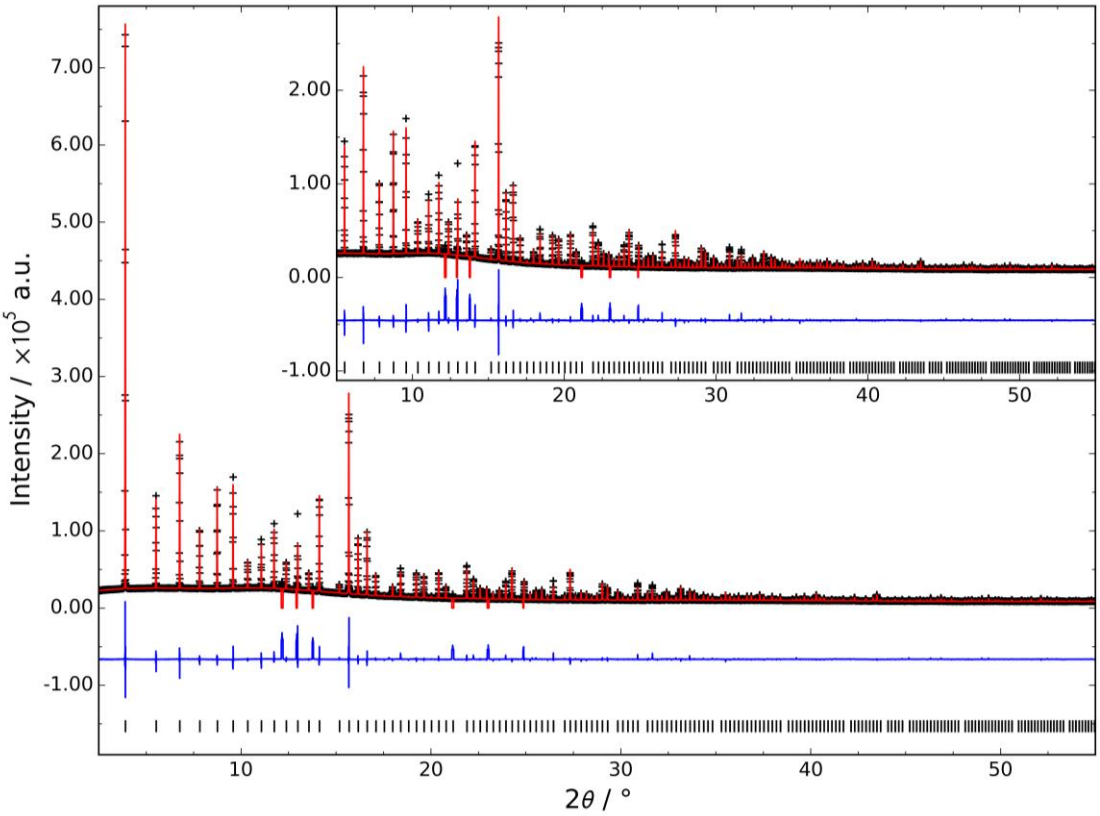

Figure S6c. Observed (black), refined (red), and difference (blue) X-Ray diffraction profiles measured for ZIF-8-98 loaded with N_2 at 1.3486 bar.

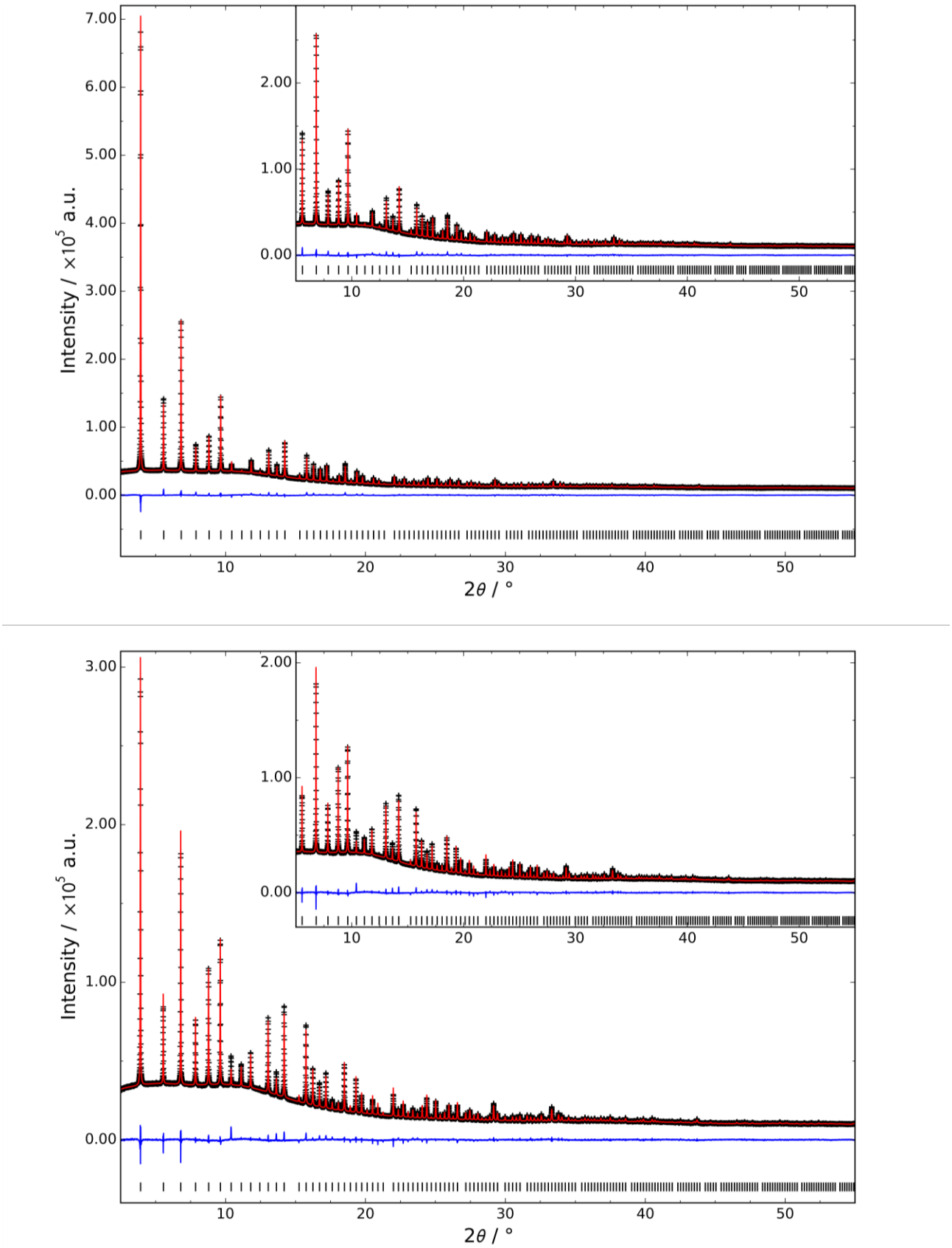

Figure S6d. Observed (black), refined (red), and difference (blue) X-Ray diffraction profiles measured for **(top)** empty ZIF-8-0.14, and **(bottom)** ZIF-8-0.14 loaded with N_2 at 0.0847 bar.

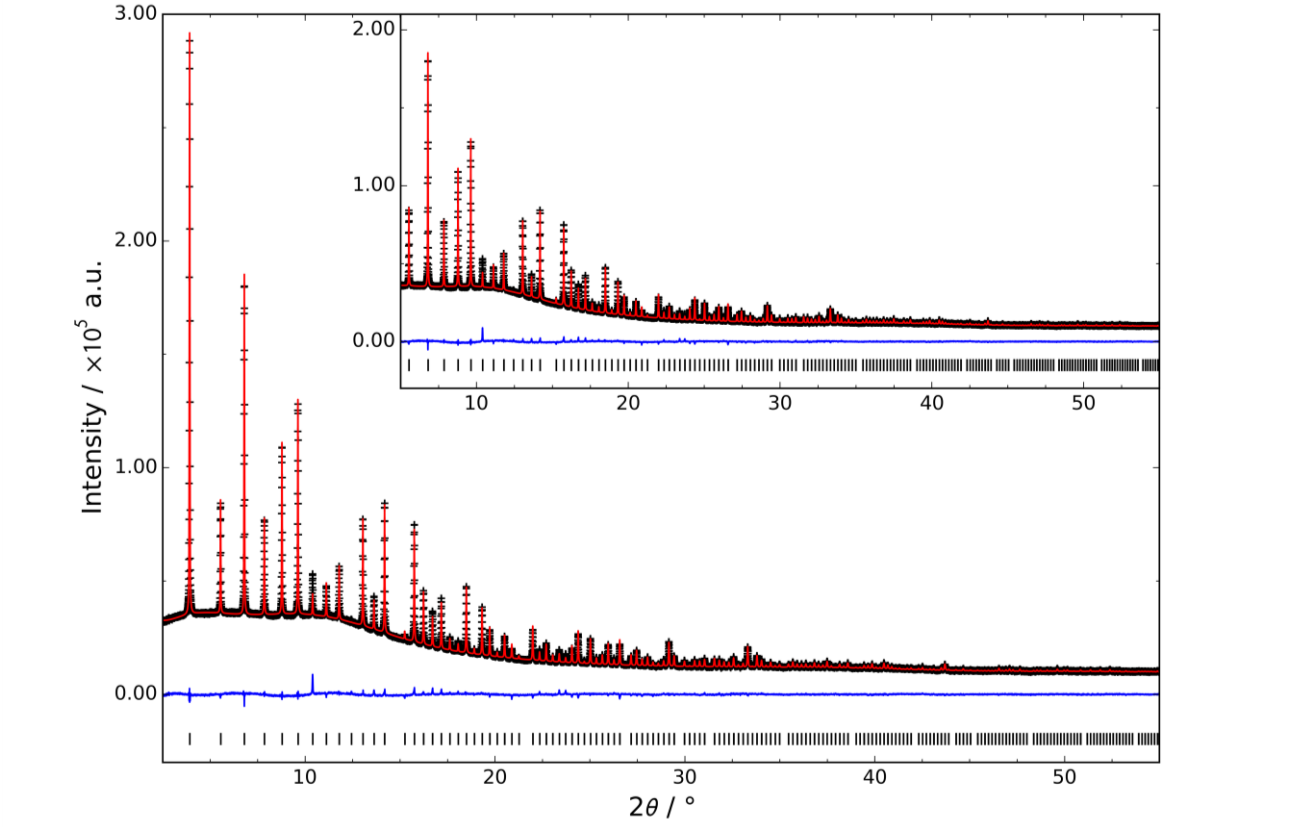

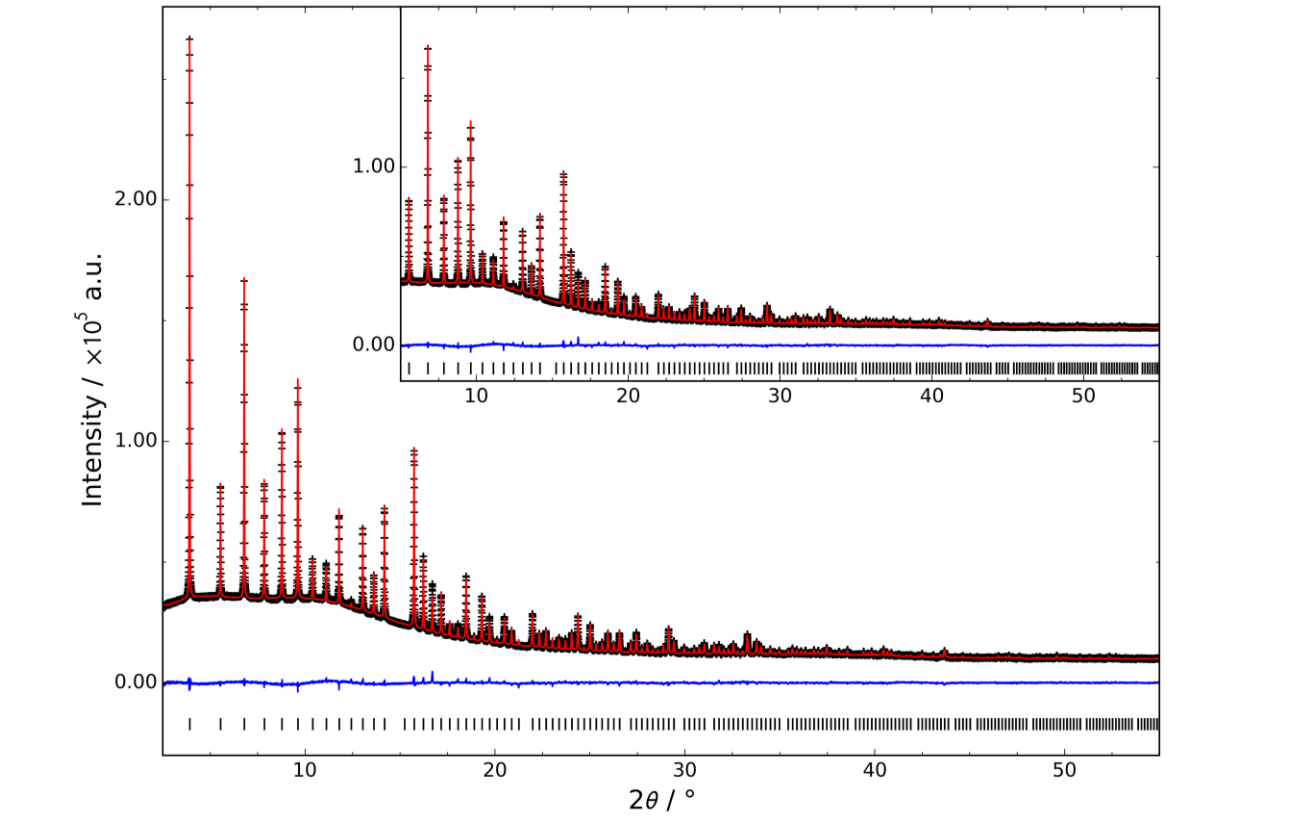

Figure S6e. Observed (black), refined (red), and difference (blue) X-Ray diffraction profiles measured for **(top)** ZIF-8-0.14 loaded with N_2 at 0.0927 bar, and **(bottom)** ZIF-8-0.14 loaded with N_2 at 0.4576 bar.

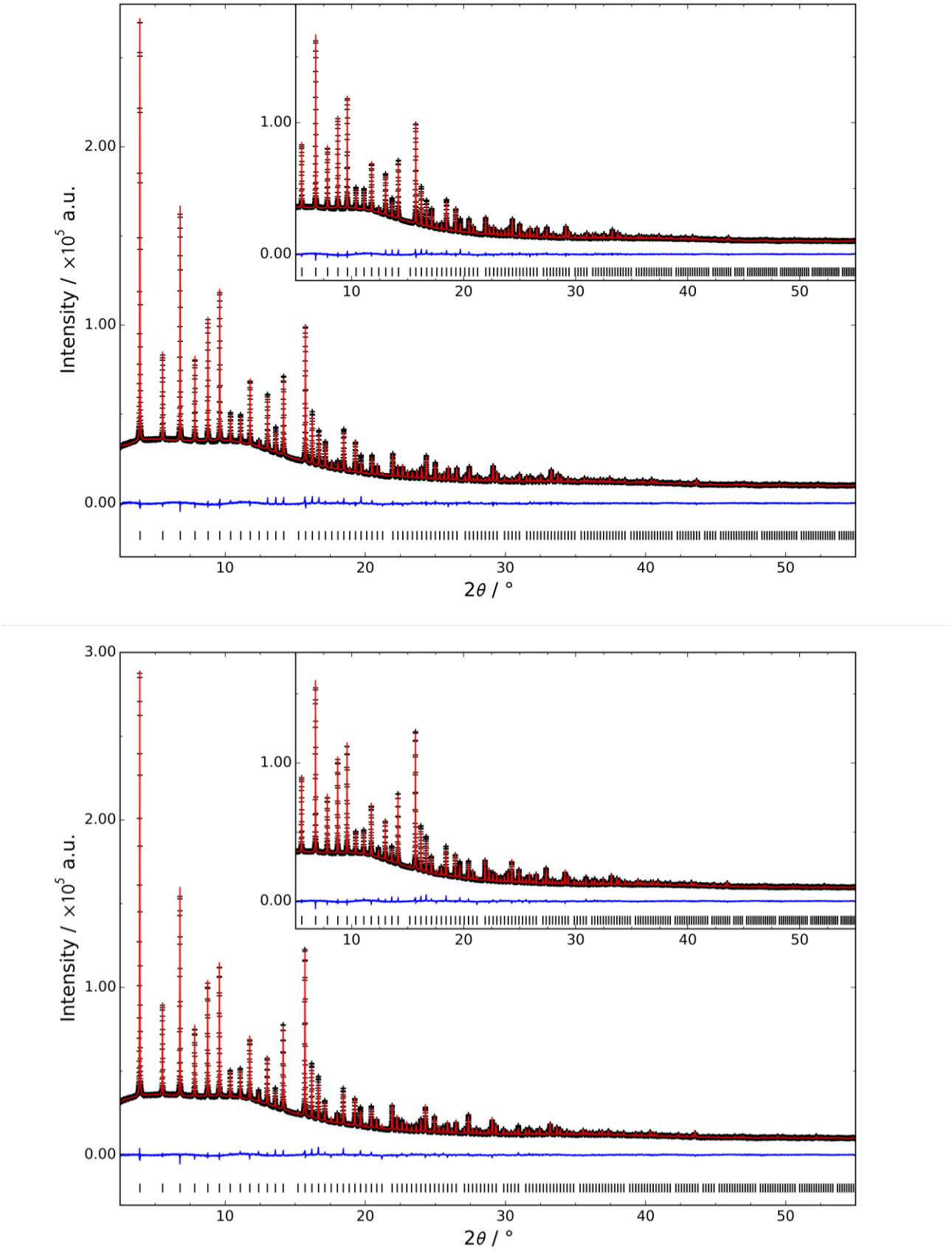

Figure S6f. Observed (black), refined (red), and difference (blue) X-Ray diffraction profiles measured for **(top)** ZIF-8-0.14 loaded with N_2 at 0.6364 bar, and **(bottom)** ZIF-8-0.14 loaded with N_2 at 0.3580 bar.

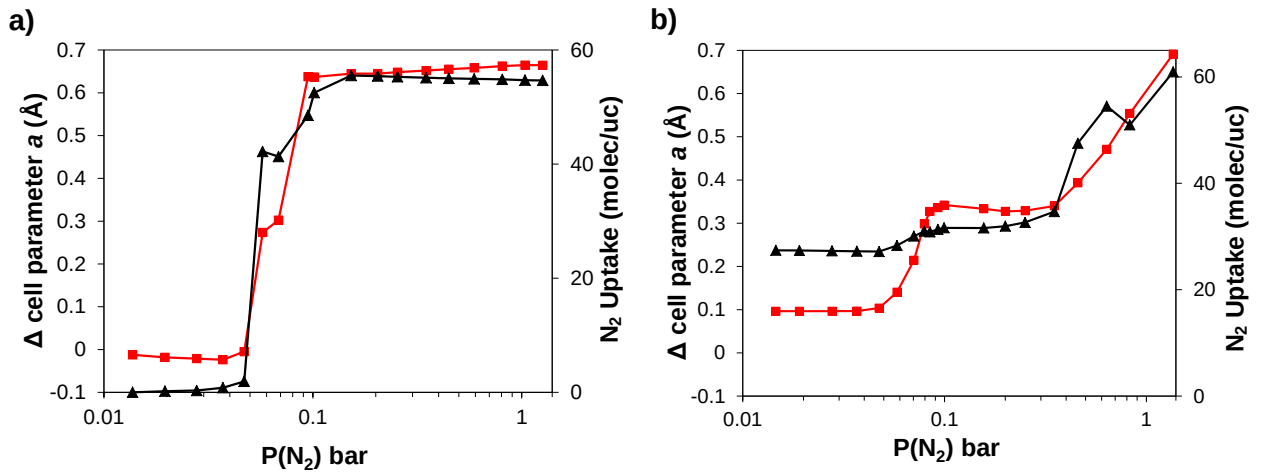

Fig. S7. Change in *a* cell parameters (red squares) along with the amount of adsorbed N_2 molecules (black triangles) at different $p(N_2)$ for **a)** ZIF-8-98 and **b)** ZIF-8-0.14.

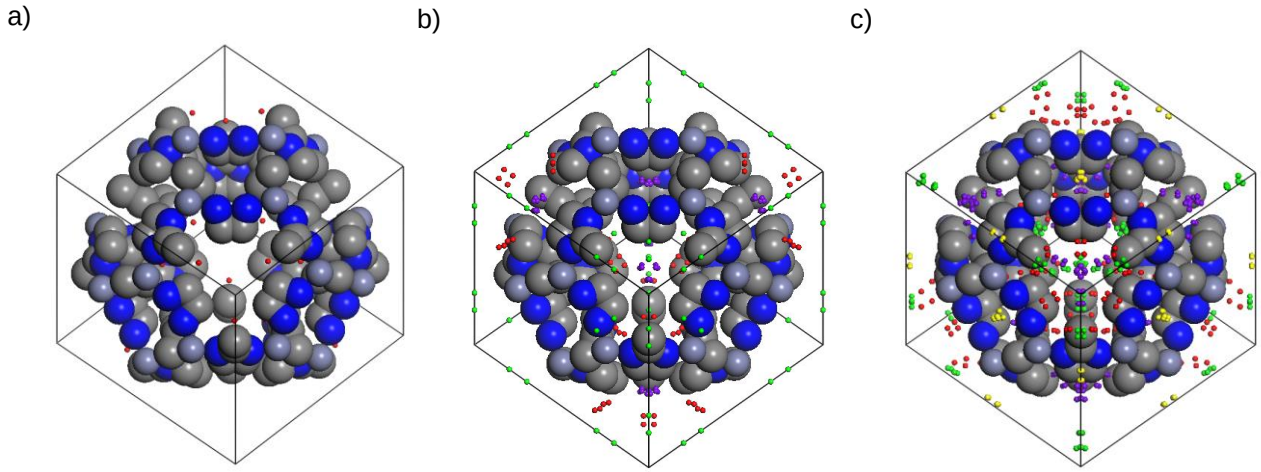

Fig. S8. Adsorption sites of N_2 at 80 K on ZIF-8-98 at **a)** 0.0469 bar; **b)** 0.068 bar; **c)** 1.3486 bar. Grey, carbon atoms; blue, nitrogen atoms; cyan, zinc atoms; red, N_2 molecules adsorbed at site I; purple, N_2 molecules adsorbed at site II; green, N_2 molecules adsorbed at site III; yellow, N_2 molecules adsorbed at site IV.

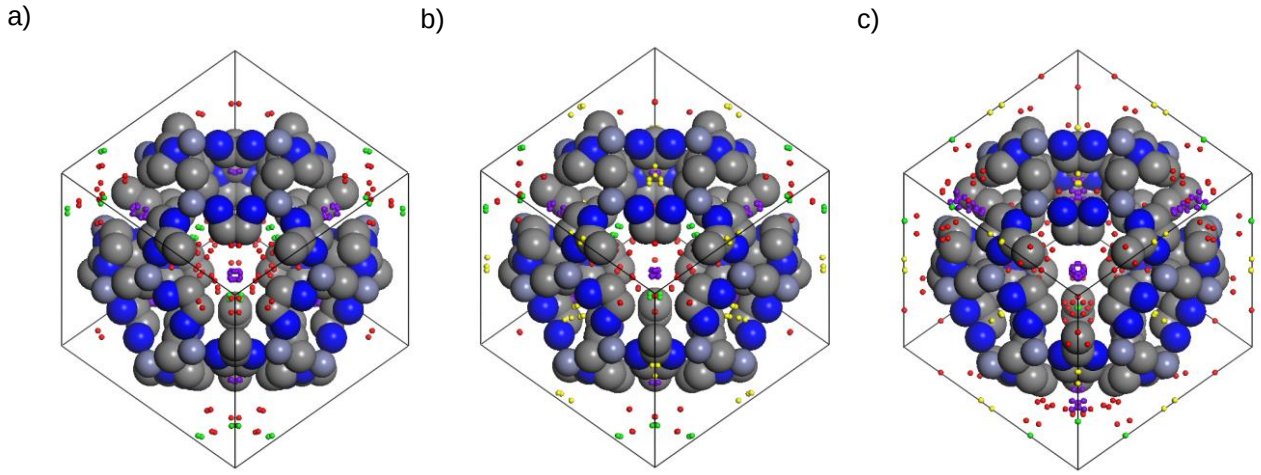

Fig. S9. Adsorption sites of N_2 at 80 K on ZIF-8-0.14 at **a)** 0.0146 bar; **b)** 0.35 bar; **c)** 1.3580 bar. Grey, carbon atoms; blue, nitrogen atoms; cyan, zinc atoms; red, N_2 molecules adsorbed at site I; purple, N_2 molecules adsorbed at site II; green, N_2 molecules adsorbed at site III; yellow, N_2 molecules adsorbed at site IV.

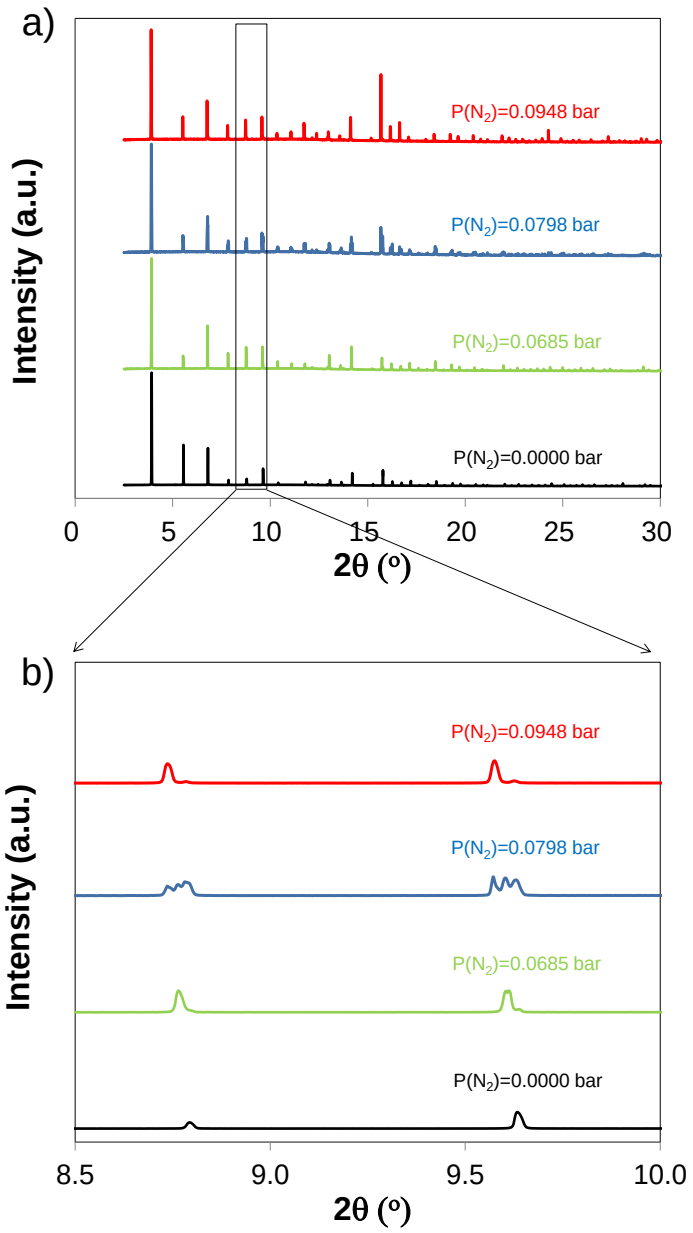

Fig. S9. In situ XRD of ZIF-8-98 at different N_2 pressure.

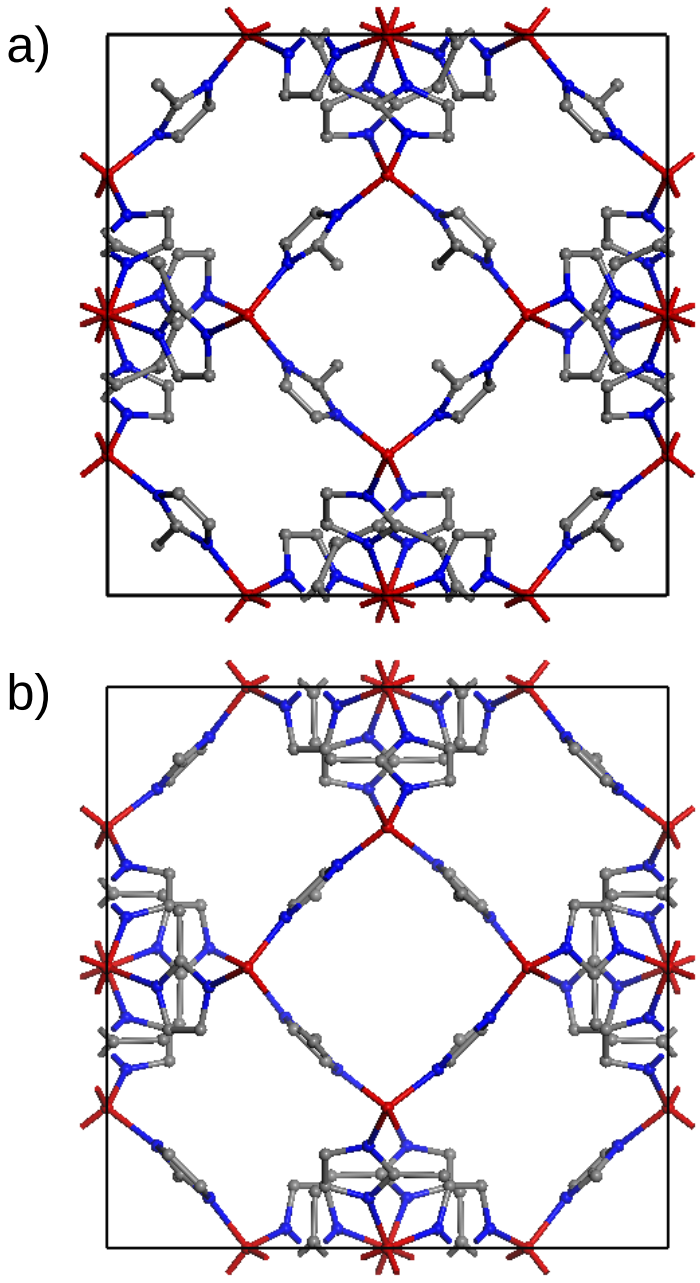

Fig. S10. Unit cell of ZIF-8-98 at a) $p(N_2)$ = 0.0000 bar, b) $p(N_2)$ = 1.3468 bar. Grey spheres, carbon; blue spheres, nitrogen; red spheres, zinc.

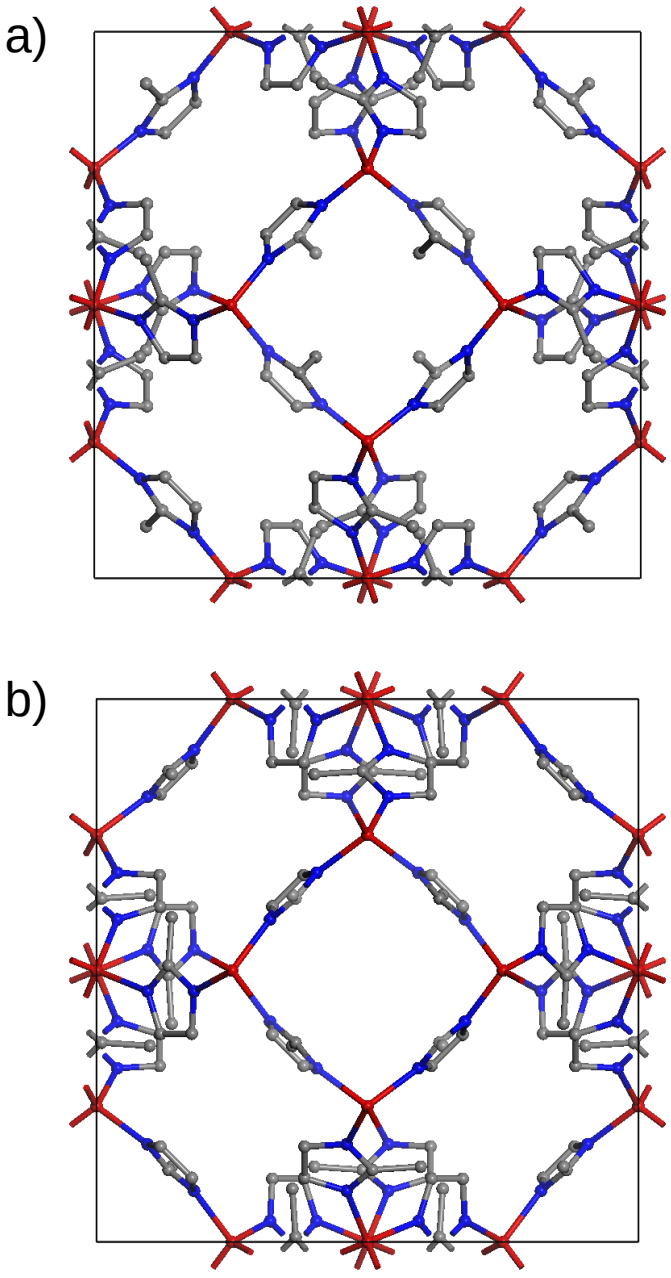

Fig. S11. Unit cell of ZIF-8-0.14 at a) $p(N_2)$ = 0.0000 bar, b) $p(N_2)$ = 1.3580 bar. Grey ball, carbon; blue ball, nitrogen; Red ball, zinc.

S7 References

1. F. Rouquerol, J. Rouquerol, K. S. W. Sing, P. Llewellyn, G. MaurinP, Adsorption by powders and porous solids. Academic Press, San Diego, 2nd edn., 2014.
2. C. O. Ania, E. García-Pérez, M. Haro, J. J. Gutiérrez-Sevillano, T. Valdés-Solís, J. B. Parra, and S. Calero, *J. Phys. Chem. Lett.*, 2012, **3**, 1159–1164.1. C. Zhang, J. a. Gee, D. S. Sholl, and R. P. Lively, *J. Phys. Chem. C*, 2014, 140821150523001.
3. J. E. Parker, J. Potter, S. P. Thompson, A. R. Lennie, and C. C. Tang, *Mater. Sci. Forum*, 2012, **706-709**, 1707–1712.
4. S. P. Thompson, J. E. Parker, S. J. Day, A. Evans, and C. C. Tang, *Eur. Astron. Soc. Publ. Ser.*, 2012, **58**, 225–229.
5. S. P. Thompson, J. E. Parker, J. Marchal, J. Potter, A. Birt, F. Yuan, R. D. Fearn, A. R. Lennie, S. R. Street, and C. C. Tang, *J. Synchrotron Radiat.*, 2011, **18**, 637–648.
6. S. P. Thompson, J. E. Parker, J. Potter, T. P. Hill, a. Birt, T. M. Cobb, F. Yuan, and C. C. Tang, *Rev. Sci. Instrum.*, 2009, **80**.
7. E. W. Lemmon, M. O. McLinden, and D. G. Friend, in *NIST Chemistry WebBook*, eds. P. J. Linstrom and W. G. Mallard, National Institute of Standards and Technology, Gaithersburg MD, 20899, USA.
8. A. Coelho, *TOPAS-Academic v5*, Coehlo Software, Brisbane, Australia, 2012.
9. S. A. Moggach, T. D. Bennett, and A. K. Cheetham, *Angew. Chemie Int. Ed.*, 2009, **48**, 7087–7089.
10. D. Fairen-Jimenez, S. A. Moggach, M. T. Wharmby, P. A. Wright, S. Parsons, and T. Düren, *J. Am. Chem. Soc.*, 2011, **133**, 8900–8902.